Hdac4 Interactions in Huntington's Disease Viewed Through the Prism of Multiomics

Authors

Joel D. Federspiel, Todd M. Greco, Krystal K. Lum, and Ileana M. Cristea

Correspondence

icristea@princeton.edu

In Brief

The histone deacetylase Hdac4 is known to contribute to the progression of Huntington's Disease (HD), but the underlying mechanisms remain unknown. Here, we defined the endogenous interactome of Hdac4 in the brain of HD mouse models, characterizing their polyQ- and age-dependence in affected tissues. Further integration with proteome and transcriptome data sets reveals the disease-induced enhancement of Hdac4 interactions with vesicular sorting proteins, including the WASH complex. This may contribute to the known decreased synaptic functions in Huntington's Disease.

Graphical Abstract

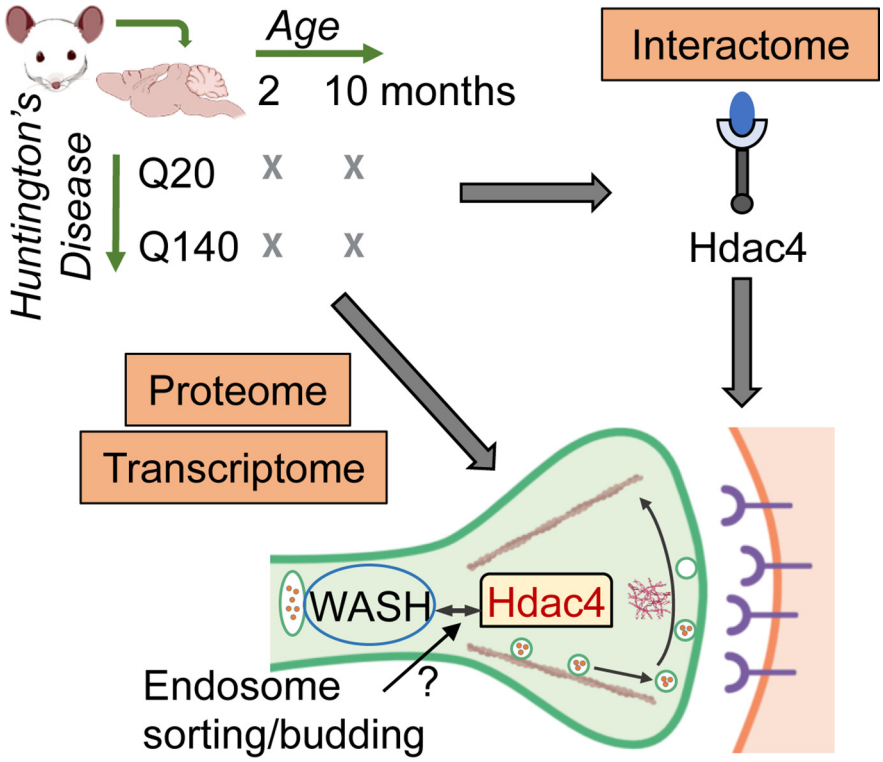

Highlights

- Endogenous interactomes of Hdac4 and Hdac5 in mouse whole brain and striata.
- Hdac4 exhibits polyQ- and age-dependent interactions in Huntington's Disease models.
- Hdac4 associates with vesicular trafficking proteins, including the WASH complex.
- Multiomics analysis supports functional Hdac4 interactions in Huntington's Disease.

Federspiel et al., 2019, Molecular & Cellular Proteomics *18*, S92–S113

https://doi.org/10.1074/mcp.RA118.001253

Hdac4 Interactions in Huntington's Disease Viewed Through the Prism of Multiomics*[S]

Joel D. Federspiel‡, Todd M. Greco‡, Krystal K. Lum‡, and Ileana M. Cristea‡§

Huntington's disease (HD) is a monogenic disorder, driven by the expansion of a trinucleotide (CAG) repeat within the huntingtin (Htt) gene and culminating in neuronal degeneration in the brain, predominantly in the striatum and cortex. Histone deacetylase 4 (Hdac4) was previously found to contribute to the disease progression, providing a potential therapeutic target. Hdac4 knockdown reduced accumulation of misfolded Htt protein and improved HD phenotypes. However, the underlying mechanism remains unclear, given its independence on deacetylase activity and the predominant cytoplasmic Hdac4 localization in the brain. Here, we undertook a multiomics approach to uncover the function of Hdac4 in the context of HD pathogenesis. We characterized the interactome of endogenous Hdac4 in brains of HD mouse models. Alterations in interactions were investigated in response to Htt polyQ length, comparing mice with normal (Q20) and disease (Q140) Htt, at both pre- and post-symptomatic ages (2 and 10 months, respectively). Parallel analyses for Hdac5, a related class IIa Hdac, highlighted the unique interaction network established by Hdac4. To validate and distinguish interactions specifically enhanced in an HD-vulnerable brain region, we next characterized endogenous Hdac4 interactions in dissected striata from this HD mouse series. Hdac4 associations were polyQ-dependent in the striatum, but not in the whole brain, particularly in symptomatic mice. Hdac5 interactions did not exhibit polyQ dependence. To identify which Hdac4 interactions and functions could participate in HD pathogenesis, we integrated our interactome with proteome and transcriptome data sets generated from the striata. We discovered an overlap in enriched functional classes with the Hdac4 interactome, particularly in vesicular trafficking and synaptic functions, and we further validated the Hdac4 interaction with the Wiskott-Aldrich Syndrome Protein and SCAR Homolog (WASH) complex. This study expands the knowledge of Hdac4 regulation and functions in HD, adding to the understanding of the molecular underpinning of HD phenotypes. ***Molecular & Cellular Proteomics 18: S92–S113, 2019. DOI: 10.1074/mcp.RA118.001253.***

Huntington's disease (HD)[1] is an inherited neurodegenerative disorder that affects about 10 in every 100,000 individuals of European ancestry (1). HD usually manifests as an adult-onset disease with progressive deficits in motor coordination and cognitive functions (2). The neuropathological phenotypes of HD are characterized by selective loss of medium spiny neurons in the striatum, and to a lesser extent, pyramidal neurons in the cortex (3). In contrast to most neurodegenerative diseases, the etiology of HD is monogenic, caused by a trinucleotide CAG repeat expansion in exon 1 of the huntingtin (*Htt*) gene (4). This expansion results in a mutant protein (mHtt) with an expanded tract of glutamine (polyQ) residues. The number of polyQ repeats is inversely correlated with age of onset of the disease symptoms (5). For example, in individuals that have mutant Htt containing 40–50Q, age of onset is usually in mid-life, whereas individuals with a juvenile age of onset may have upwards of 250 Q residues. The expanded polyQ tract of mHtt increases its self-aggregation and propensity to form oligomers and eventually insoluble aggregates (6–8).

In contrast, HD disease progression is less correlated with polyQ length (9) and the development of symptoms can be patient-specific. Moreover, despite the observed selectivity of HD neurodegeneration, the root-cause pathogenic protein, mHtt, is widely expressed in most tissues. Taken together, this suggests that although HD etiology is monogenic, HD pathophysiology is multifactorial. Indeed, mHtt is known to have pleotropic effects on "omics" cellular networks, exerting significant polyQ-dependent effects on the transcriptome (10–13) and proteome (13). In both human and mouse HD models, down-regulation of specific genes is observed, largely because of decreased transcription from gene promoters (14–16). As a result, cellular factors that modulate gene expression and chromatin states, such as histone acetyltransferases and lysine deacetylases, have been the subject of intense investigation (17). Moreover, the lysine acetyltransferase CREB-binding protein (CBP) has been found to co-localize with huntingtin inclusions (18), whereas histone deacetylase interaction partners were found to have altered subcellular distribution patterns in HD brains (19). Because one of the primary roles of lysine deacetylases is transcriptional repression, the relevance of these enzymes to HD pathophysiology is an active area of research (20). Broad

From the ‡Department of Molecular Biology, Princeton University, Washington Road, Princeton, New Jersey 08544
Received December 2, 2018, and in revised form, March 27, 2019
Published, MCP Papers in Press, April 30, 2019, DOI 10.1074/mcp.RA118.001253

spectrum inhibition of lysine deacetylases has been found to ameliorate HD-related phenotypes in R6/2 transgenic mice, which was also associated with degradation of specific histone deacetylases, Hdac2 and Hdac4 (21).

Given the family of Hdacs are ascribed to unique subclasses, in part stemming from their distinct cellular functions (22), pharmacological and molecular manipulation of specific Hdacs have been further pursued as potential avenues for intervention (23, 24). The observed degradation of Hdac4 after inhibitor treatment of HD mice has prompted several studies investigating its potential role in HD pathogenesis (21). Hdac4 is a class IIa lysine deacetylase that shuttles between the nucleus and cytoplasm (25). In the nucleus, Hdac4 functions as a transcriptional regulator through interaction with corepressors (26). Yet surprisingly, direct reduction of Hdac4 levels did not affect transcriptional dysfunction linked to mHtt and did not alter nuclear huntingtin aggregation in HD mouse models (23). Instead, it led to a reduction in cytoplasmic Htt aggregates and the overall improvement of HD-related phenotypes (23). Consistent with this observation, Hdac4 appears to be largely cytoplasmic in the brain and has been reported to physically interact with mutant huntingtin (Htt) in the cytoplasm of mouse neurons (23, 27). Yet, the underlying molecular mechanisms that convey improved HD phenotypes with reduced Hdac4 levels are not known. One aspect of Hdac4 biology that has not been sufficiently studied in the brains of HD or non-affected animal models, particularly with unbiased experimental approaches, is the regulation of its protein interactions. Although studies of Hdac4 interactions isolated from cell culture models have been performed, usually via epitope-tagged Hdac4 (28), endogenous Hdac4-containing protein complexes have not been studied in tissues.

To address this limited understanding of Hdac protein interactions and their relevance to HD pathophysiology, we undertook a systems level study of Hdac4 in the whole brain and striatum of HD mouse models with normal (Q20) and mutant (Q140) Htt at pre-symptomatic and symptomatic ages. To explore the modulation of endogenous Hdac4 interactions, we pursued an immunoaffinity purification-mass spectrometry (IP-MS) approach. Because there are no prior reports of IP-MS studies of endogenous Hdac4 in any tissues, this study required an initial extensive optimization of an experimental workflow for the efficient solubilization and enrichment of endogenous Hdac4 from brain tissues. To discover interactions underlying specific Hdac4 functions, we performed parallel interaction studies of endogenous Hdac5, a related class IIa Hdac that was found not to have an impact on HD phenotypes. Overall, our results identified specific molecular targets that have known roles in synaptic plasticity and vesicle trafficking. These enriched functional associations with Hdac4 coincided with an overall dysregulation of synaptic processes in the Q140 HD mouse models, as we determined by integration of proteome and transcriptome data sets from striata of the same HD mouse series, further strengthening the relevance of Hdac4 in HD. More broadly, these results expand the knowledge of Hdac4 regulation and functions in the context of HD and may provide a framework for understanding the molecular underpinning of HD phenotypes and for designing therapeutic interventions.

[1] The abbreviations used are: HD, huntington's disease; IP-MS, immunoaffinity purification mass spectrometry; Hdac4, histone deacetylase 4; Hdac5, histone deacetylase 5; Htt, huntingtin; TBS, tris-buffered saline; TBST, TBS plus 0.1% tween-20; HINT, huntingtin INTeraction database; PCA, principal component analysis.

EXPERIMENTAL PROCEDURES

Animal Models—Animal lines used were Strain 370504 HttQ20 Heterozygous males and Strain 400809 Q140 neo delete Heterozygous males at ~8 and 40 weeks of age. Animals were raised and sacrificed at The Jackson Laboratory (Bar Harbor, Maine) in compliance with their Institutional Animal Care and Use Committees (IACUC), and whole brains and dissected striata were provided as flash frozen tissue.

Western Blotting for IP Optimization and Evaluation—Western blot analysis of bait solubilization and IP efficiency was performed to evaluate isolation and IP performance. Equal percentages of input, pellet, and flowthrough and 2% of the elution were loaded onto 4–12% Bis-Tris gels (Thermo Fisher Scientific, Waltham, MA). Following SDS-PAGE, proteins were electrophoresed onto PVDF membranes overnight at 40V constant voltage. Following this, membranes were blocked in 5% milk in tris-buffered saline (TBS) for one hour at room temperature. Membranes were then exposed to primary antibody in 5% milk in TBS plus 0.1% tween-20 (TBST) according to the following: Hdac4 - H9536 (Sigma Aldrich, St. Louis, MO), 1:2000 dilution, 2 h room temperature; Hdac5 - sc-133225 (Santa Cruz Biotechnology, Dallas, TX), 1:250 dilution, 2 h room temperature, GAPDH - 5174S (Cell Signaling Technology, Danvers, MA). Membranes were washed 3 times with TBST and then exposed to secondary antibody in 5% milk in TBST for 45 min at room temperature. Secondary antibodies (goat anti-rabbit A-21109 and goat anti-mouse A-21058, Fisher Scientific) both conjugated to Alexafluor 680 were used at a 1:10,000 dilution. Westerns were imaged on the LI-COR Odyssey CLx system (LI-COR Biosciences, Lincoln, NE) using automatic settings.

Immunoaffinity Purification of Endogenous Hdacs From Whole Brain or Striata—Before IP, antibodies were pre-conjugated to magnetic protein A/G beads (Thermo Fisher Scientific, 88802) for 1 h at 4 °C in 20 mM K-HEPES pH 7.4, 110 mM KOAc, 2 mM $MgCl_2$, 0.1% Tween-20, 1 μM ZnCl2, 1 μM $CaCl_2$. For whole brain IPs, 50 μg of each antibody was conjugated to a 50 μl slurry of beads. For striatum IPs, 25 μg of each antibody was conjugated to 25 μl slurry of beads. Following the 1 h incubation, beads were washed 3 $\times$ 500 μl in IP wash buffer (buffer 19): 10 mM HEPES, pH 7.4, 1% Triton X-100, 0.1% Tween-20, 0.2% Sodium Deoxycholate, 150 mM NaCl, 2 mM $CaCl_2$, 3 mM KCl, 2 mM $MgSO_4$, 1.2 mM NaH_2PO_4.

IPs were performed from either whole brains or dissected striata. For this, the tissues were first lysed in buffer 19 supplemented with 1:100 dilution of HALT protease and phosphatase inhibitor (Thermo Fisher Scientific, 78446), and 1:2500 dilution of universal nuclease (Thermo Fisher Scientific, 88700). For the whole brain experiments, one brain was lysed in 40 ml of buffer and split into three IPs (Hdac4, Hdac5, IgG). For the striatum experiments, 9 striata were pooled and lysed together in 20 ml of buffer and then split into three IPs (Hdac4, Hdac5, IgG). In both cases, the brain tissue was minced on ice and then lysed in 5 ml of buffer by homogenizing in a tenbroeck homog-

enizer for 20 strokes on ice. The homogenized tissue was transferred to the remaining lysis buffer and incubated on ice for 5 min and then spun down at 8000 × *g* for 10 min at 4 °C to separate the insoluble material. Protein concentrations were assessed by BCA assay (Thermo Fisher Scientific, 23225) and adjusted for equal loading across IPs. For whole brain IPs, isolations were performed on 14 mg of protein and for striatum IPs, isolations were performed on 7 mg of protein. The concentration adjusted soluble protein was aliquoted into three tubes for IP using either IgG or antibodies against endogenous Hdac4 or Hdac5 for 1 h at 4 °C with rotation.

Following the 1 h incubation, the beads were accumulated using a magnet and then resuspended in 1 ml of IP wash buffer and transferred to a 2 ml round bottom tube. The beads were then washed with 3 × 1 ml of IP wash buffer, resuspended in 1 ml of cold ddH_2O and transferred to a new 2 ml round bottom tube. Beads were washed once more with 1 ml of cold ddH_2O and then eluted in 85 μl of 106 mM Tris HCl, 141 mM Tris base, 2% LDS, 0.5 mM EDTA at 70 °C for 10 min. Beads were magnetically separated from the eluted proteins (supernatant) and the eluted proteins were then transferred to a new 1.5 ml tube and mixed with 25 mM TCEP (Thermo Fisher Scientific, 20491) and 50 mM chloroacetamide and incubated at 70 °C for 20 min. Proteins were then digested by FASP (29–31) and peptides were fractionated in three fractions by StageTip (32) as previously described (33).

Reciprocal IP and Western Blot Analysis—Interactions with the Wiskott-Aldrich Syndrome Protein and SCAR Homolog (WASH) complex were evaluated by reciprocal IP in HEK-293T cells. A construct containing HDAC4-GFP was subcloned from (28) and placed into a pEGFP-N1 vector. WASH complex components Washc3 and Washc5 and the accessory protein Snx27 were cloned from mouse cDNA generously provided by Dr. Yibin Kang (Princeton University, Princeton, NJ) into a pcDNA5–3X FLAG vector generously provided by Dr. Ralph Kleiner (Princeton University, Princeton, NJ). Wash1 was subcloned from Addgene plasmid #55163, which was a gift from Michael Davidson. Additionally, full length WASHc2 and the first 220 amino acids of WASHc2 (enough for interactions with Wash1, Washc3, Washc4, and Washc5) were cloned from human cDNA into pcDNA5–3X FLAG. Cloning was performed by PCR using either KOD Hot Start DNA polymerase (Sigma Aldrich, 71086–3) or Phusion HF DNA polymerase (New England Biolabs, M0530L) according to the manufacturer's instructions. Primers used for all cloning steps are listed in supplemental Table S1. HDAC4-GFP was co-transfected into a 70% confluent 10 cm dish of HEK-293T cells with either a FLAG-tagged WASH complex component or empty FLAG vector using XtremeGene HP DNA transfection reagent (Sigma Aldrich, 6366244001) according to the manufacturer's instructions. One day post transfection, cells were harvested and lysed in lysis buffer 19 and homogenized by Polytron (Kinematica) at 25,000 rpm for 20 s. Following pelleting of insoluble material, FLAG IPs with 10 μg of antibody were performed using the same protocol described for Hdac IPs above. Reciprocal isolation of HDAC4-GFP with the FLAG-tagged WASH constructs was assessed using Western blotting as described above. Antibodies used were: FLAG (F1804, Sigma Aldrich) 1:4000, 1 h room temperature; GFP (11814460001, Roche) 1:2000, 1 h room temperature; Hdac4 - H9536 1:2000, 1 h room temperature.

LC-MS/MS Analysis—Following peptide fractionation, label-free samples were analyzed on an Ultimate 3000 nanoRSLC coupled online with an ESI-LTQ-Orbitrap Velos ETD mass spectrometer (Thermo Electron, San Jose, CA). Reverse-phase chromatography was performed over a 20 cm IntegraFrit column (IF360–75-50-N-5, New Objective, Woburn, MA) packed in-house with 1.9 μm ReproSil-Pur C18-AQ (Dr. Maisch, GmbH) with mobile phase A: 0.1% formic acid in water and mobile phase B: 0.1% formic acid in 97% acetonitrile. Peptides were separated over a 150 min gradient (5% B to 30% B) with 250 nl/min flow rate and analyzed by MS1 survey scans followed by data-dependent collision-induced dissociation (CID) MS/MS fragmentation of top 15 most abundant ions. The following parameters were used: FT preview scan disabled, waveform injection and dynamic exclusion enabled, automatic gain control target value of 1×10^6 for MS and 1×10^4 for ion trap MS/MS scans, max ion injection time of 300 ms for MS and 125 ms for MS/MS scans. For MS scans: *m/z* range of 350–1700 and resolution of 120,000; for MS/MS scans: minimum signal of 1,000, isolation width of 2.0, normalized collision energy of 30% and activation time of 10 ms.

Mass Spectrometry Informatics—MS/MS spectra were searched against a FASTA file containing mouse protein sequences and common contaminants (16,932 sequences, download 7/2016 from Uniprot) using Proteome Discoverer 2.2.0.388. The Spectrum Files RC node and Minora Feature Detector nodes were used to perform offline mass recalibration and label-free MS1 quantitation respectively. Specifically, to minimize false propagation of MS/MS identifications, we utilized the Minora feature detection algorithm in Proteome Discoverer 2.2, which performs mass recalibration, retention time alignment, and propagation of features confirmed by MS/MS. After mass recalibration and feature alignment, the optimal settings for retention time and mass tolerance windows are determined by Minora based on the distribution of mass accuracy and RT variance. We then assessed the overall linear regression fits of the matching algorithm by examining landmark features for each file to ensure that the mapping was reasonable. We additionally spot-checked several peptides for different abundance levels.

The data were searched using Sequest HT with settings for a fully tryptic search with a maximum of two missed cleavages, precursor mass tolerance of 5 ppm, fragment mass tolerance of 0.3 Da, static carbamidomethylation of cysteine, dynamic oxidation of methionine, dynamic deamidation of asparagine, dynamic loss of methione plus acetylation of the protein N terminus, and dynamic phosphorylation of serine, threonine, and tyrosine. A reverse database search was also performed to determine FDR. The matched spectra were then passed to the Percolator node to perform PSM validation and then to the ptmRS node for PTM site localization assignment.

A consensus file was then created in Proteome Discoverer 2.2 for each data set using the Feature Mapper and Precursor Ions Quantifier nodes. The MS1 signals were mapped across runs to pick up missing values from peptides not sequenced in every run and then quantified by taking the max peak intensity for each peptide. The precursor ion quantifier node was set to leave normalization and scaling off. Additionally, the merge mode of the MSF file node was set to "per file and search engine type" and the target false discovery rate (FDR) (Strict) settings in the Peptide Validator node were set to 0.01. These settings preserve the spectral count data from each sample and set the FDR to 1% respectively. For protein inference, two unique peptide sequences were required. Only unique and razor peptides were used for MS1 quantitation.

Bioinformatic Analysis of Interaction Data—The assembled data set was inspected for quality and then exported to excel for further analysis. Total spectral count data was analyzed by SAINT (34) using the REPRINT (35) interface. SAINT was run with LowMode off, MinFold on, and Normalize on and the average SAINT score from the best two replicates in each condition was used for specificity assessment. The selection of appropriate SAINT score thresholds was based on both our previous assessment of suitable SAINT scores when studying interactions of the different eleven HDACs (HDAC1-HDAC11) (28), and on examination of our current interaction data from the brain tissues. Specifically, like our previous human HDAC4 interactome study in CEM T cells, we used a SAINT score cutoff of ≥0.8 for isolations of Hdac4 in the whole brain for the Q20 2- and 10-month data and the Q140 2-month data (28). For the Q140 10-month data,

we observed an overall increase in the number of proteins that passed this cutoff. Given the possibility that some of these interactions may derive non-specifically from the increased aggregation present in these symptomatic brains, we used a more stringent cutoff of ≥0.95 when analyzing these data. For the Hdac5 isolations in whole brain, a uniform threshold of ≥0.7 was applied for all conditions. In the striatum, there was an increase in the number of high-scoring proteins when compared with the whole brain IPs; however, no differential effect of the symptomatic mice was observed on the number of high scoring proteins. Therefore, a uniform cutoff of ≥0.95 was used for Hdac4 in all striatum conditions. For Hdac5 isolations in the striatum, we again used a uniform cutoff of 0.7 in all conditions.

Proteins passing specificity thresholds were further analyzed in a variety of ways using MS1 abundance-based quantitation, which includes values gained from feature matching. Network interaction diagrams incorporating relative quantitation and known protein-protein interaction data were generated in Cytoscape (36) using information and enrichments from STRING (37). The ClueGO (38) app in Cytoscape was used to perform different sets of two-group comparisons of enriched proteins and interactions. Heatmaps of the quantitative MS1 data were generated using Morpheus (Broad Institute, https://software.broadinstitute.org/morpheus). Principal component analysis (PCA) was conducted using the Clustvis (39) resource. Information on known Htt-interacting proteins was retrieved from the Huntingtin INTeraction (HINT) database (www.hdinhd.org). For heatmap and Cytoscape network visualization, interacting proteins were normalized to their respective bait proteins in each IP and the median of the three replicate value was used. Parts of some figures were generated using https://biorender.io under an academic license.

Multiomic Investigation of Striatum from HD Model Mice—The transcriptome data was obtained from supplemental Table 1 in (13) and used without further modification. The whole proteome data on the same mice was generated on a Q Exactive instrument platform and was downloaded from PRIDE (PXD006302) in RAW format and researched in Proteome Discoverer 2.2 using similar settings as described above with the following exceptions: the Sequest HT search was performed with a precursor mass tolerance of 5 ppm and 0.02 Da mass error on the fragment ions; no phosphorylations were included in this search, all other modifications listed previously were included. MS1-based label free quantitation was again performed, and the samples were normalized to the total peptide signal in each replicate. Imputation of missing values was performed only when a peptide was detected in at least half (four) of the replicates analyzed and the imputed value was generated from a normal distribution around the median of the detected values. Quantitative evaluation was performed by pairwise comparisons of all detected peptides and the median ratio was used for protein level comparison. Significance assessment was performed using the background-based ANOVA method implemented in Proteome Discoverer 2.2 and multiple comparison adjustment of the *p* values was performed. A minimum of two unique peptides and quantitation in at least half of the samples was required for further evaluation of each protein.

Proteome data was mapped to transcriptome data by converting protein accession numbers to Entrez gene IDs using the Retrieve/ID mapping tool of uniprot.org. For all accessions that could not be mapped to an Entrez gene ID, the gene symbol was used to map against the transcriptome data set. The final set of protein-mRNA pairs considered for analysis consisted of those proteins that mapped unambiguously to either an Entrez Gene ID or to a gene name in the transcriptome set. This resulted in a final set of 7939 genes for which protein and RNA measurements were available. Comparisons of the proteome and transcriptome were performed by assessing significantly differential gene products (adjusted *p* value ≤0.1) and $\log_2$ fold change values of Q140/Q20 mice at each age (2 and 10 months). For the construction of Gene Ontology/Pathway heatmaps, the ontology terms associated with each protein were downloaded from the UniProt KnowledgeBase (release 2018–10). The associated terms and corresponding proteome and transcriptome relative abundance were imported into the Perseus software (40). Using the individual transcript and protein relative abundances, an average relative abundance was calculated for each ontology/pathway term that contained at least 3 annotated proteins. Heatmaps were constructed separately for each ontology/pathway, and clustered by Euclidean distance and average linkage using the $\log_2$-transformed average relative abundances in Morpheus.

Experimental Design and Statistical Rationale—IPs of Hdac4 and Hdac5, along with IgG controls, were performed from whole brain tissue and dissected striatum in biological triplicate. For the whole brain IPs, one single brain was used for each replicate of IPs (Hdac4, Hdac5, and IgG). For the striatum IPs, 9 individual striatum were pooled before lysis to have enough material for one replicate of IPs. In each case, the triplicate IPs were performed from four different experimental conditions (Q140 and Q20 mice at 2 and 10 months of age) for a total of 72 IPs analyzed in total. This sample size was chosen to provide sufficient statistical power for analysis while minimizing the number of animals needed for the experiments. The same IgG control from each condition was used as a negative control for both the Hdac4 and Hdac5 isolations to determine specificity. The previously generated whole proteome and transcriptome data sets used for dissected striatum were performed with 8 replicates each as described in (13). SAINT specificity score assessments were performed as described (34). All enrichment analyses were multiple comparison adjusted within the respective software used to perform the analysis and adjusted *p* values of ≤0.05 were considered significant. For comparison of proteome and transcriptome, a multiple comparison adjusted *p* value threshold of ≤0.1 was used to provide a more complete comparison, consistent with (13). Statistical comparisons of interaction level trends were performed in Prism using the Kruskal-Wallis test.

RESULTS

Optimization of Endogenous Hdac4 Isolation from Brain Tissue—To investigate the means through which Hdac4 plays a role in HD, we sought to determine the interactome of Hdac4 in a relevant HD model system. For this, we used a mouse model that heterozygously expresses a human exon 1 of Htt with the rest of the Htt sequence being from mouse (Fig. 1*A*). This system is available as an allelic series with varying numbers of CAG repeats (and thus polyQ lengths), thereby providing models for normal (low polyQ) and HD disease (high polyQ) conditions. In agreement with previous literature (13, 41), the Q20 mouse was used as a "normal" condition, as this repeat length represents a non-disease causing polyQ repeat, and the Q140 mouse represented an HD disease condition. To further place the knowledge of Hdac4 interactions in the context of age, we performed interaction studies in normal- or HD-mice of 2 and 10 months of age, representing a pre-symptomatic and a post-symptomatic age, respectively.

We first had to begin our investigation by performing a series of optimizations for the IP of Hdac4 (Fig. 1*A*). Before this study, to our knowledge, no other study has reported an IP-MS of endogenous Hdac4 from brain tissue or another type of tissue. Despite the availability of commercial anti-Hdac4 antibodies, many of these antibodies proved to either

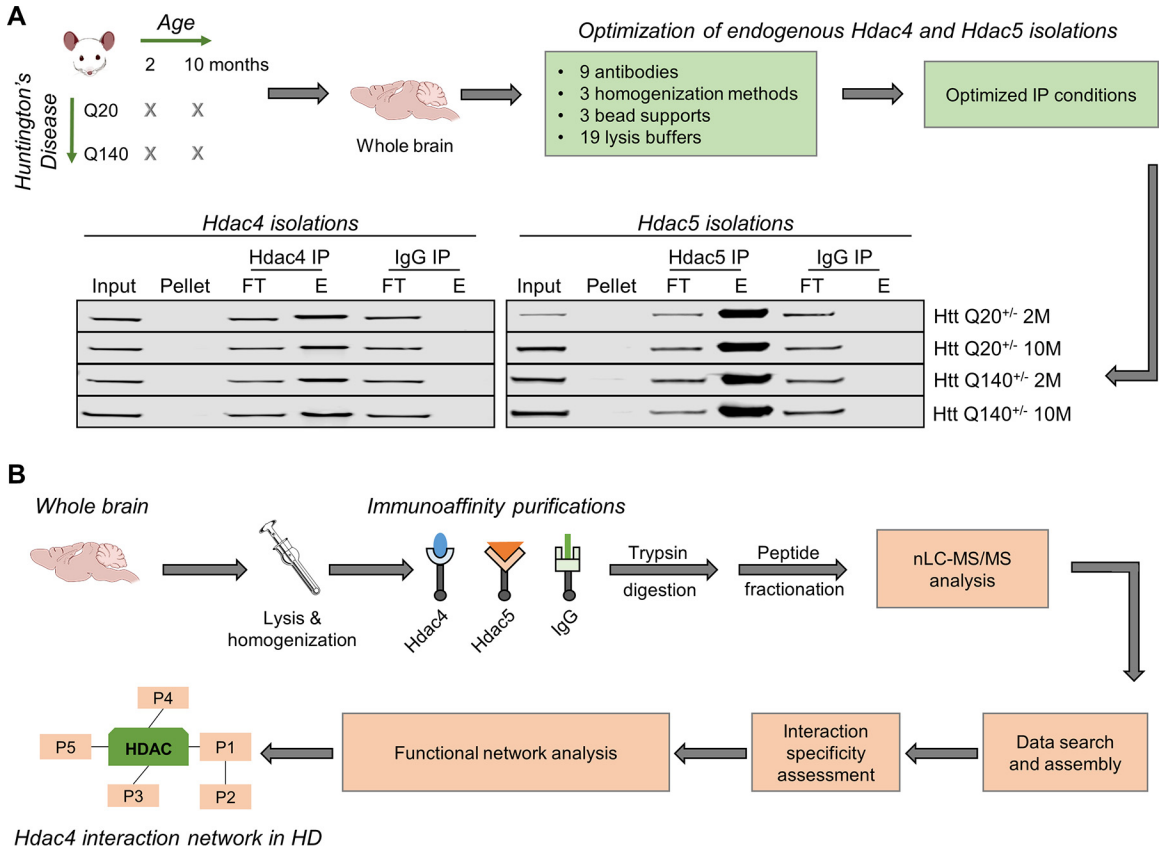

FIG. 1. **Optimization workflow for the analyses of endogenous Hdac4 and Hdac5 interaction in the brain of HD mouse models.** *A*, Isolations of endogenous Hdacs were optimized in whole mouse brain lysates. Multiple antibodies and buffers were tested to arrive at an optimized set of conditions demonstrated in the Western blotting. *B*, Using the optimized isolation conditions, IPs of Hdac4 and Hdac5, along with IgG controls, were performed from whole brain, analyzed by LC-MS/MS, filtered for interaction specificity, and bioinformatically assessed for known interactions and functional enrichments.

lack enough affinity or specificity. For example, we found one of the antibodies to have stronger cross-reactivity for Gja1 rather than for Hdac4. In total, we tested five different antibodies against endogenous Hdac4, which allowed us to identify the one best suited for immunoaffinity purification. The isolation method was further refined by comparing three different homogenization methods, Dounce, cryogenic lysis and polytron homogenization. As cryogenic lysis usually provides an effective and reproducible lysis for experiments using cells (42), we tested several different lysis buffers using this homogenization method (supplemental Table S2, supplemental Fig. S1*A*). However, the lysis buffers that solubilized Hdac4 and Hdac5 were too harsh for the antibodies to work effectively for IP and still did not fully solubilize other proteins to the extent expected. Therefore, we next tested Dounce-based homogenization and found the solubilization of the Hdacs in brain tissue much improved (supplemental Fig. S1*B*).

Next, as the composition of the lysis buffer has a profound effect on the maintenance and specificity of the identified protein interactions (42), we continued to fine-tune the performance of the IPs by comparing six additional lysis buffers (supplemental Table S2, supplemental Fig. S1*C*). In each additional buffer, we evaluated solubilization of bait proteins, efficiency of bait capture, and overall background binding to arrive at an optimal set of conditions for all three parameters while maintaining interactions. In parallel with these optimizations, we also tested three different bead isolation systems including antibodies covalently coupled to M270 Dynabeads (ThermoFisher) or FG beads (Nacalai) and antibodies non-covalently coupled to magnetic protein A/G beads (Thermo Fisher). The non-covalently coupled magnetic protein A/G beads proved to have the best antibody binding affinity and lowest background binding of the bead supports tested.

Ultimately, we arrived at an optimal set of conditions for the efficient isolation of endogenous Hdac4 from mouse brain tissue (Fig. 1*A*, Western blotting). As controls, we performed parallel immunoaffinity purifications of IgG, as well as of endogenous Hdac5 (Fig. 1*B*). As another class IIa histone deacetylase, Hdac5 also shuttles between the nucleus and the cytoplasm and is known to share interactions with Hdac4 (28). However, unlike Hdac4, Hdac5 has not been found to have a role in HD disease (23). Therefore, the comparison of endogenous Hdac4 and Hdac5 interactions would allow us to distinguish interactions that are unique to Hdac4 and poten-

tially relevant in HD. The isolation of Hdac5 also required optimization, and we tested four antibodies before selecting the best for IP studies. Using our optimized lysis and isolation conditions, we generated functional interaction networks by performing three biological replicate IP-MS analyses for both Hdac4 and Hdac5 from Q20 and Q140 mouse brain at 2 and 10 months of age (Fig 1*B*).

Hdac4 Interactions in Whole Brain Reveal an Association with RNA Binding and Vesicle Trafficking Proteins—To begin analyzing our IP-MS data sets we used our negative control IgG isolation data and the SAINT algorithm to assign specificity scores to the identified proteins. It should be noted that although the IgG controls and SAINT filtering help to eliminate proteins that associate non-specifically with the beads or antibodies used, there is still a possibility that some of the proteins identified can derive from the cross-reactivity of the antibody and not interaction with Hdac4 or Hdac5. On examining the score distributions, we assigned a specificity cutoff for Hdac4 of ≥0.8 for the Q20 2- and 10-month data and the Q140 2-month data, a score in line with that previously used for human HDAC4-FLAG IP from CEM T cells (28). We assigned a cutoff of ≥0.95 for the Hdac4 Q140 10-month data owing to the increased number of high scoring interactions in this data set (supplemental Table S3). On examining the specificity-filtered Hdac4 interactions, the enrichment in cytoplasmic proteins was evident and in agreement with the known localization of Hdac4 in brain tissue (23, 27) (Fig 2*A*). Only a small number of chromatin related proteins were detected in our Hdac4 IP.

To ensure that our lysis and isolation conditions are not biasing the results against previously reported nuclear Hdac4 interactions, we performed an additional IP experiment. We used our previously generated HDAC4-GFP expressing CEM-T cells and immunoaffinity purified HDAC4-GFP using the same lysis conditions as for our brain sample with either anti-GFP antibodies or the antibody against endogenous HDAC4. As we expected for CEM-T cells, where HDAC4 has both prominent nuclear and cytoplasmic localization, we identified its known functional interactions with nuclear proteins, including NCOR1 and TBL1XR1 (supplemental Fig. S2). Therefore, this combination of resin, antibody and lysis condition is effective for isolating HDAC4 and its interactions regardless of their subcellular localization. Adding further confidence to the cytoplasmic localization of Hdac4 in brain tissue, we also compared the relative levels of phosphorylated Hdac4 at Ser629 (pSer629, Ser632 in human), which is known to be a 14–3-3 interaction site required for Hdac4 shuttling to the cytoplasm. Normalized to total Hdac4 isolated, we observed over 400-fold increases in pSer629 levels in the brain samples when compared with T-cells (Fig 2*B*) (28). Having confirmed that our method was not biasing against the detection of known Hdac4 nuclear interactions, we proceeded to further investigate the functional classes of the interactions observed in brain tissue.

Among the identified Hdac4 associations were those with RNA binding proteins and proteins involved in phosphoinositide (PI) signaling, neuronal function and vesicle trafficking (Fig 2*A*). Interestingly, PCA analysis of Hdac4 interactions did not reveal any overt trends driven by age or Q length (Fig 2*C*). However, a comparison of the relative abundances (based on MS1 peak-area label-free quantitation) of these interactions did show a slight decreasing trend with both age and Q length (Fig 3*A*). Of note, this trend was not influenced by the differential selection of SAINT score cutoff for the Q140 10-month sample when compared with the other IPs, as a similar trend was observed when using ≥0.8 SAINT scores for all Hdac4 IPs (supplemental Fig. S3). Further assessment of these age- and Q-dependent changes revealed clusters of decreasing and increasing associations within distinct functional groups (Fig. 3*B*).

The RNA binding proteins grouped into four distinct abundance profiles (Fig 3*B*) as shown in the line plots. Individual proteins in the highlighted groups are shown in heatmaps below the line plots. Group 1 exhibited a slight increase in Hdac4 association in the Q140 mice with little age-dependent change. Group 2 RNA binding proteins, on the other hand, did not change their associations with Hdac4 in a Q length-dependent manner, but had an evident age-dependent decrease in association. These proteins include RNA-binding protein with serine-rich domain 1 (Rnps1) and RNA-binding protein 39 (Rbm39) that are involved in mRNA splicing (43). Group 3 exhibited both and age and Q length-dependent decrease in association. Included in this group are the proteins Zinc finger RNA-binding protein (Zfr) and Staufen homolog 2 (Stau2). Zfr has been reported to control the cytoplasmic localization of Stau2 (44), which transports RNA from the cell body to the dendrite. Group 4 retained similar associations with Hdac4 at all conditions, except for an increase at 10 months of age in the Q20 animals. The ribosomal and translation-associated proteins had a trend of decreased associations with both age and Q length, whereas the polysome proteins only exhibited an age-related decrease in Hdac4 association. It should be noted that ribosome proteins are frequently identified in IP-MS data sets as possible nonspecific associations. Given their relative enrichment compared with control isolations, it is possible that these represent specific Hdac4 associations in this biological context. Altogether, this Hdac4 association with RNA binding proteins and proteins associated with cytosolic ribosomes, polysomes, and translation, could suggest and involvement for Hdac4 in post-transcriptional regulation in mouse brain.

The Hdac4 association with cytoplasmic proteins could also be divided into three main abundance profiles groups (Fig 3*B*). Of interest are the groups that contained either interactions that increased with age or decreased with polyQ length (groups 2 and 3, respectively). Group 3 contained proteins involved in cytoskeletal regulation, including sorting

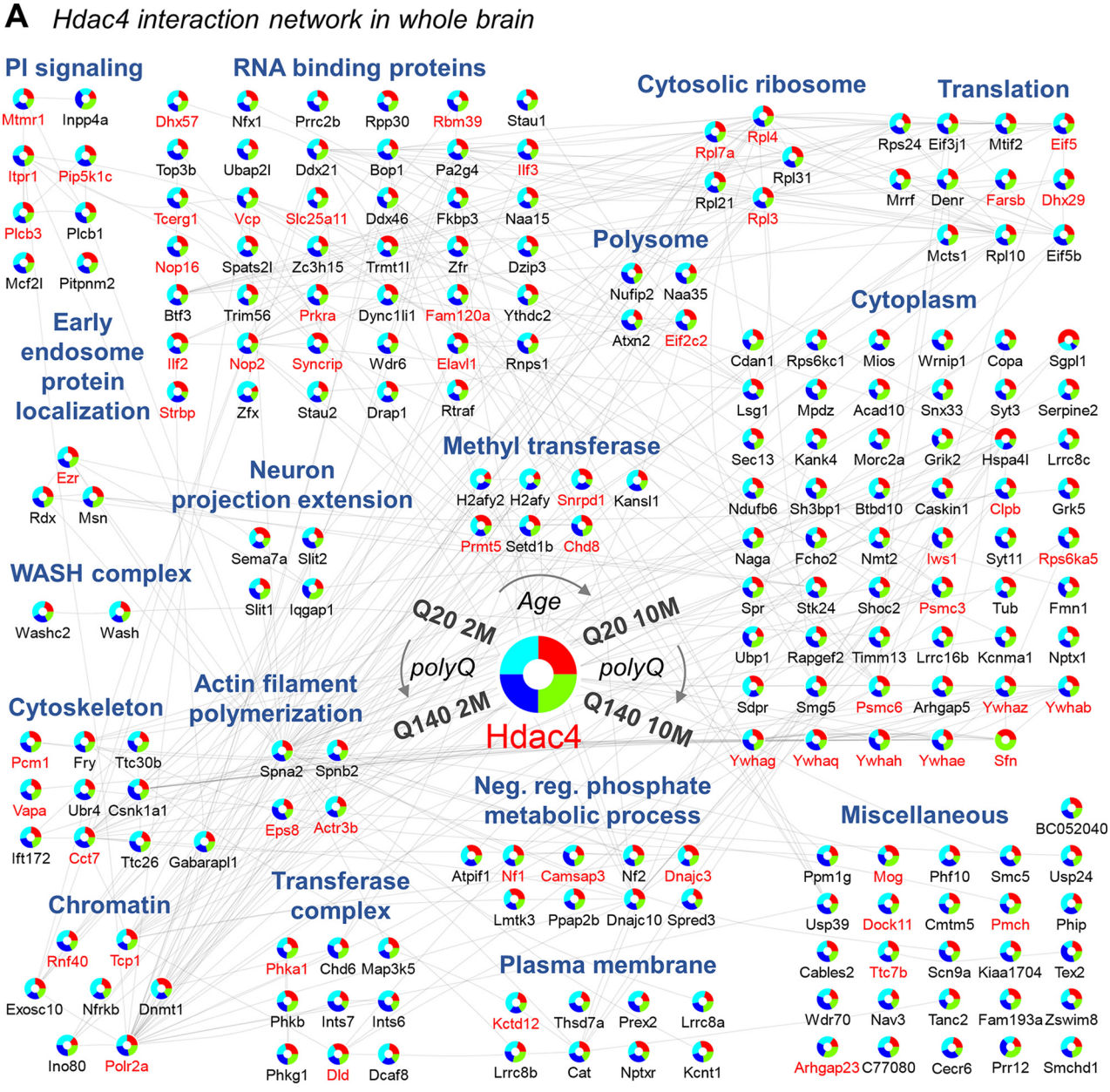
A
Hdac4 interaction network in whole brain
PI signaling
Mtmr1
Inpp4a
Itpr1
Pip5k1c
Plcb3
Plcb1
Mcf2l
Pitpnm2
RNA binding proteins
Dhx57
Nfx1
Prrc2b
Rpp30
Rbm39
Stau1
Top3b
Ubap2l
Ddx21
Bop1
Pa2g4
Ilf3
Tcerg1
Vcp
Slc25a11
Ddx46
Fkbp3
Naa15
Nop16
Spats2l
Zc3h15
Trmt1l
Zfr
Dzip3
Btf3
Trim56
Prkra
Dync1li1
Fam120a
Ythdc2
Ilf2
Nop2
Syncrip
Wdr6
Elavl1
Rnps1
Strbp
Zfx
Stau2
Drap1
Rtraf
Cytosolic ribosome
Rpl4
Rpl7a
Rpl31
Rpl21
Rpl3
Translation
Rps24
Eif3j1
Mtif2
Eif5
Mrrf
Denr
Farsb
Dhx29
Mcts1
Rpl10
Eif5b
Polysome
Nufip2
Naa35
Atxn2
Eif2c2
Cytoplasm
Cdan1
Rps6kc1
Mios
Wrnip1
Copa
Sgpl1
Lsg1
Mpdz
Acad10
Snx33
Syt3
Serpine2
Sec13
Kank4
Morc2a
Grik2
Hspa4l
Lrrc8c
Ndufb6
Sh3bp1
Btbd10
Caskin1
Clpb
Grk5
Naga
Fcho2
Nmt2
Iws1
Syt11
Rps6ka5
Spr
Stk24
Shoc2
Psmc3
Tub
Fmn1
Ubp1
Rapgef2
Timm13
Lrrc16b
Kcnma1
Nptx1
Sdpr
Smg5
Psmc6
Arhgap5
Ywhaz
Ywhab
Ywhag
Ywhaq
Ywhah
Ywhae
Sfn
Early endosome protein localization
Ezr
Rdx
Msn
Neuron projection extension
Sema7a
Slit2
Slit1
Iqgap1
Methyl transferase
H2afy2
H2afy
Snrpd1
Kansl1
Prmt5
Setd1b
Chd8
WASH complex
Washc2
Wash
Age
Q20 2M
Q20 10M
polyQ
polyQ
Q140 2M
Q140 10M
Hdac4
Cytoskeleton
Pcm1
Fry
Ttc30b
Vapa
Ubr4
Csnk1a1
Ift172
Cct7
Ttc26
Gabarapl1
Actin filament polymerization
Spna2
Spnb2
Eps8
Actr3b
Neg. reg. phosphate metabolic process
Atpif1
Nf1
Camsap3
Nf2
Dnajc3
Lmtk3
Ppap2b
Dnajc10
Spred3
Miscellaneous
BC052040
Ppm1g
Mog
Phf10
Smc5
Usp24
Usp39
Dock11
Cmtm5
Pmch
Phip
Cables2
Ttc7b
Scn9a
Kiaa1704
Tex2
Wdr70
Nav3
Tanc2
Fam193a
Zswim8
Arhgap23
C77080
Cecr6
Prr12
Smchd1
Chromatin
Rnf40
Tcp1
Exosc10
Nfrkb
Dnmt1
Ino80
Polr2a
Transferase complex
Phka1
Chd6
Map3k5
Phkb
Ints7
Ints6
Phkg1
Dld
Dcaf8
Plasma membrane
Kctd12
Thsd7a
Prex2
Lrrc8a
Lrrc8b
Cat
Nptxr
Kcnt1
B
Hdac4 phosphorylation (pSer 629/632)
FC > 400
Relative abundance
0.04
0.03
0.02
0.01
0.00
Q20 2M
Q20 10M
Q140 2M
Q140 10M
T cells
C
PCA of Hdac4 interactions in whole brain
PC2 (13.7%)
PC1 (53.1%)
20
10
0
-10
-20
-40
-20
0
20
40
Q length
Q20
Q140
Age
2M
10M

nexin-33 (Snx33) (45) and KN motif and ankyrin repeat domain-containing protein 4 (Kank4) (46).

Perhaps of most interest was the uncovered Hdac4 association with proteins related to vesicle trafficking and neuronal function (Figs 2*A* and 3*B*). One example is the interaction with members of the Wiskott-Aldrich Syndrome Protein and SCAR Homolog (WASH) complex (47), a pentameric protein complex that functions as part of the endosomal protein sorting machinery. Specifically, WASH induces membrane bending and the localization of filamentous (F-) actin to endosomes, thereby contributing to retromer-mediated vesicle trafficking. Additionally, Hdac4 interacted with other proteins involved in driving localization to early endosomes, in the regulation of actin filaments, as well as in neuron outgrowth, thereby suggesting a potential Hdac4 role in intracellular transport or its regulation via trafficking. Further support comes from our observed association with phosphoinositol signaling proteins, known to play roles in diverse cellular pathways, including vesicle trafficking (48). On investigating the changes in these associations with age and polyQ length, we observed three different trends. However, most of these proteins displayed decreased associations with Hdac4 in the Q140 10-month mice. The exceptions were Iqgap1 and Inpp4a (group 1) that had increased associations in these mice (Fig 3*B*).

Given the previously identified functional association of Hdac4 with Htt in HD mouse models, we also asked whether any previously reported Htt-interacting proteins were present in our network. To do this, we used the Huntingtin INTeraction (HINT) database curated on hdinhd.org and compared our data set to this list of reported Htt-interacting proteins. Proteins found in HINT were labeled in red text in our interaction network (Fig 2*A*). We further examined all of the Hdac4-interacting proteins in HINT for any concerted patterns in their abundance profiles. We identified three distinct patterns (Fig 3*B*) that did not cluster along functional lines but rather were distributed throughout the functional clusters. Interestingly, the group 3 proteins showed an increased Hdac4 association with age in the Q20 mice, but not a substantial difference in association in the Q140 mice, perhaps indicating that these interacting proteins are being sequestered by Htt in the expanded polyQ mice and are therefore less available for interaction with Hdac4.

Lastly, we compared the Hdac4 interactome with that of Hdac5 in the whole brain IPs (supplemental Fig. S4, supplemental Table S4). Remarkably, these two class IIa HDACs had very different interaction networks. Although also having enriched associations with cytoplasmic proteins, Hdac5 interacts predominantly with tubulin and the centrosome, as well as with carbon metabolism proteins. In fact, aside from the 14–3-3 proteins that aid the cytoplasmic shuttling for both enzymes, only four protein interactions seem to be shared between Hdac4 and Hdac5 in the brain: Sptan1, Cat, Fry, and Pcm1. This finding contrasts with our previous findings for human HDAC4 and HDAC5 protein interactions in cultured human T cells, in which these enzymes were predominantly nuclear and shared numerous interactions (28, 49). Therefore, this observation provides further support for the notion that Hdac4 has unique functions that are distinct from Hdac5 in the mouse brain and in the context of HD.

Hdac4 Interactions in the Striatum Are Enriched in Vesicle Trafficking and Synaptic Functions—Given our finding that Hdac4 associates with vesicle transport and neuronal function proteins and that these interactions change with age and Q length, we next wanted to validate these associations and further investigate them in a brain region that is specifically affected by HD. Therefore, we performed a new series of IP-MS experiments in the HD-vulnerable brain region of striatum (50, 51), and first confirmed that the optimized IP conditions still work effectively in the striatum (supplemental Fig. S5). We then performed three biological replicate IPs of endogenous Hdac4 and Hdac5, in parallel to IgG control IPs in dissected striatum, analyzed these by mass spectrometry, and generated specificity-filtered functional interaction networks. A SAINT score of $\geq$0.95 was used for all Hdac4 IPs (supplemental Table S5). For visualization purposes, some interactions are depicted in supplemental Fig. S6. Similar to the whole brain IPs, we further overlaid information about known Htt-interacting proteins onto our interaction networks, highlighting in red text the proteins also found in the HINT database.

The striatum-specific Hdac4 interaction network has many broad similarities in protein classes and functions as those found in the whole brain interactome. However, unlike in the whole brain IPs, in the striatum we observed a stronger impact of Htt Q length on the Hdac4 interactome. In a PCA analysis of the specificity-filtered interactions, we noticed that the different Q length samples tended to cluster together (Fig 4*A*), and that age did not have a large impact on this behavior. This can also be seen in the overall distribution of the relative abundances of Hdac4 interactions in the striatum (Fig 4*B*), which differs from that in the whole brain (Fig 3*A*).

As expected from the subcellular localization of Hdac4, we again observed an enrichment of cytoplasmic proteins along with only a small number of chromatin-associated proteins. We also saw an enrichment in RNA-binding proteins, proteins associated with translational regulation, and phosphoinositol

FIG. 2. **Investigation of Hdac4 protein interaction in whole brain.** *A*, Comparison of endogenous Hdac4 interactions in Q20 and Q140 mice at 2 and 10 months of age. Each interacting protein is shown as a ring plot with the relative median MS1 abundance levels in each isolation condition depicted as indicated on the Hdac4 ring at the center of the network. Gene names shown in red are Hdac4 specific interactions that are also reported Htt interactions. Edges represent known protein-protein interactions and other associations present in the STRING database. Protein interactions have been functionally grouped and labeled in blue text. *B*, Relative Hdac4 pSer629 levels in mouse brain are over 400-fold higher than in cultured human T cells. *C*, PCA of Hdac4 interactions in whole brain shows no overt Q- or age-dependent trend.

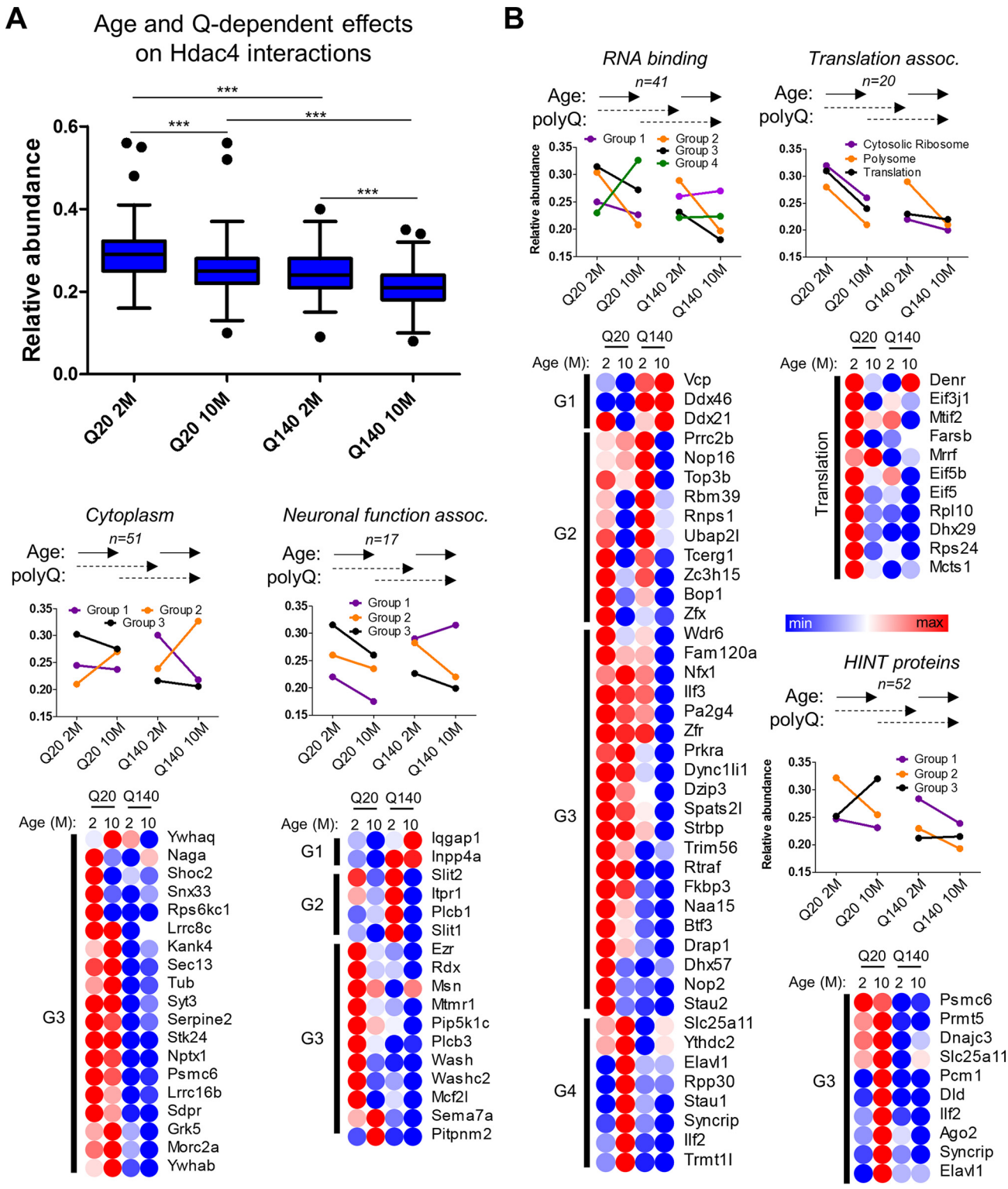

FIG. 3. **Alterations in Hdac4 whole-brain protein interactions with Htt polyQ length and age.** *A*, Line plots and heatmaps of selected interaction categories are shown. Each category is broken down into three or more groups of proteins with similar abundance profiles and these are shown on the line graphs depicting the relative association with Hdac4 (scaled 0–1) in each condition with a different color for each group. The number of proteins examined in each functional grouping is listed below the title of each. Below these graphs are heatmaps depicting all members of one or more groups shown in the line graph above. The heatmaps show the relative changes in each protein across conditions with the minimal amount associated with Hdac4 getting a blue color and the maximal association with Hdac4 a red color. *B*, A slight trend of decreased relative interaction abundances is observed across age and Q length. *** $p \leq 0.001$, Kruskal-Wallis test.

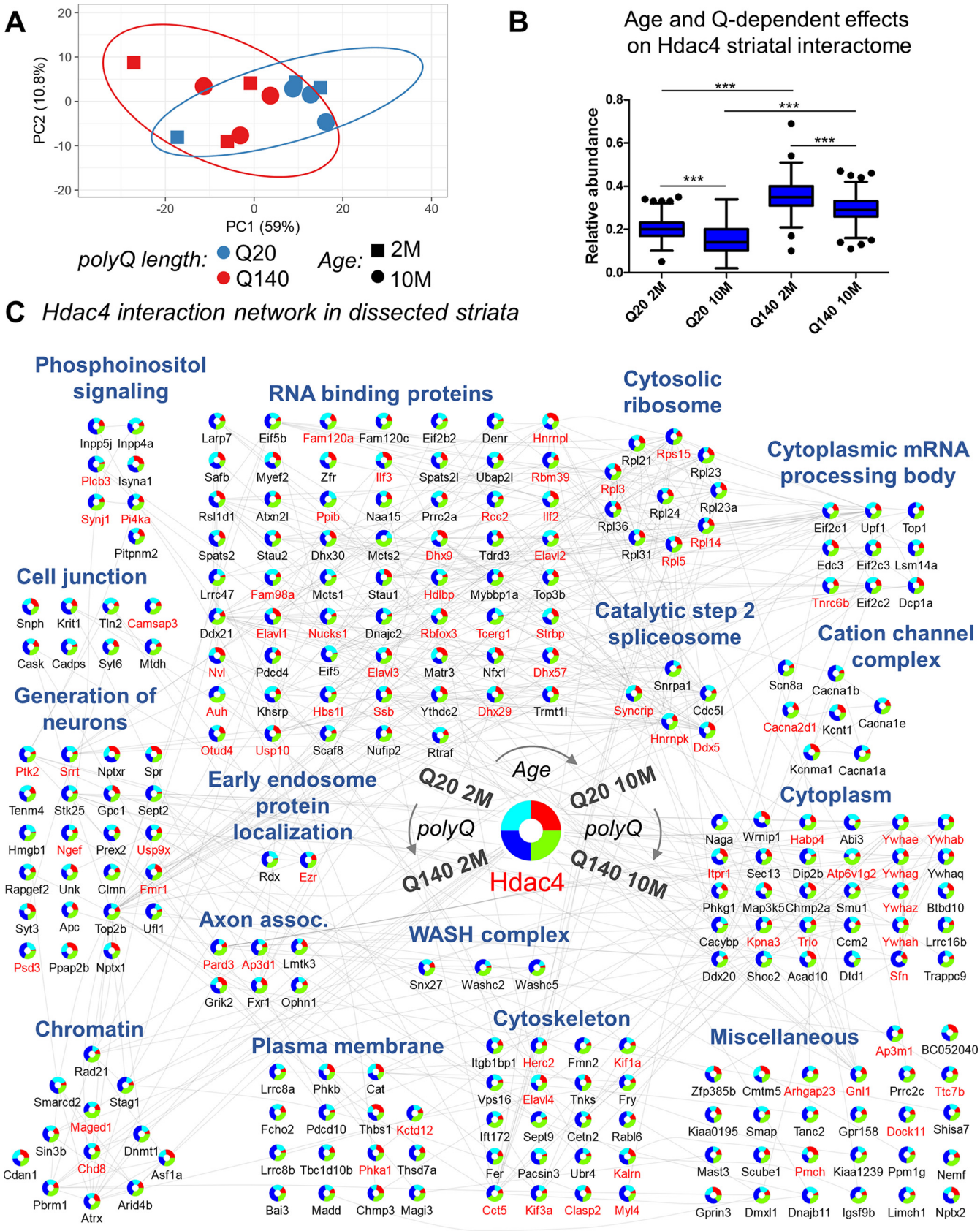
A
PC2 (10.8%)
PC1 (59%)
polyQ length: Q20 Q140
Age: 2M 10M
B
Age and Q-dependent effects on Hdac4 striatal interactome
Relative abundance
Q20 2M
Q20 10M
Q140 2M
Q140 10M
C Hdac4 interaction network in dissected striata
Phosphoinositol signaling
Inpp5j Inpp4a Plcb3 Isyna1 Synj1 Pi4ka Pitpnm2
RNA binding proteins
Larp7 Eif5b Fam120a Fam120c Eif2b2 Denr Hnrnpl Safb Myef2 Zfr Ilf3 Spats2l Ubap2l Rbm39 Rsl1d1 Atxn2l Ppib Naa15 Prrc2a Rcc2 Ilf2 Spats2 Stau2 Dhx30 Mcts2 Dhx9 Tdrd3 Elavl2 Lrrc47 Fam98a Mcts1 Stau1 Hdlbp Mybbp1a Top3b Ddx21 Elavl1 Nucks1 Dnajc2 Rbfox3 Tcerg1 Strbp Nvl Pdcd4 Eif5 Elavl3 Matr3 Nfx1 Dhx57 Auh Khsrp Hbs1l Ssb Ythdc2 Dhx29 Trmt1l Otud4 Usp10 Scaf8 Nufip2 Rtraf
Cytosolic ribosome
Rpl21 Rps15 Rpl23 Rpl3 Rpl24 Rpl23a Rpl36 Rpl14 Rpl31 Rpl5
Cytoplasmic mRNA processing body
Eif2c1 Upf1 Top1 Edc3 Eif2c3 Lsm14a Tnrc6b Eif2c2 Dcp1a
Cell junction
Snph Krit1 Tln2 Camsap3 Cask Cadps Syt6 Mtdh
Catalytic step 2 spliceosome
Snrpa1 Syncrip Cdc5l Hnrnpk Ddx5
Cation channel complex
Scn8a Cacna1b Cacna2d1 Kcnt1 Cacna1e Kcnma1 Cacna1a
Generation of neurons
Ptk2 Srrt Nptxr Spr Tenm4 Stk25 Gpc1 Sept2 Hmgb1 Ngef Prex2 Usp9x Rapgef2 Unk Clmn Fmr1 Syt3 Apc Top2b Ufl1 Psd3 Ppap2b Nptx1
Early endosome protein localization
Rdx Ezr
Age
Q20 2M
Q20 10M
polyQ
polyQ
Q140 2M
Q140 10M
Hdac4
Cytoplasm
Naga Wrnip1 Habp4 Abi3 Ywhae Ywhab Itpr1 Sec13 Dip2b Atp6v1g2 Ywhag Ywhaq Phkg1 Map3k5 Chmp2a Smu1 Ywhaz Btbd10 Cacybp Kpna3 Trio Ccm2 Ywhah Lrrc16b Ddx20 Shoc2 Acad10 Dtd1 Sfn Trappc9
Axon assoc.
Pard3 Ap3d1 Lmtk3 Grik2 Fxr1 Ophn1
WASH complex
Snx27 Washc2 Washc5
Chromatin
Rad21 Smarcd2 Stag1 Maged1 Sin3b Dnmt1 Chd8 Cdan1 Asf1a Pbrm1 Arid4b Atrx
Plasma membrane
Lrrc8a Phkb Cat Fcho2 Pdcd10 Thbs1 Kctd12 Lrrc8b Tbc1d10b Phka1 Thsd7a Bai3 Madd Chmp3 Magi3
Cytoskeleton
Itgb1bp1 Herc2 Fmn2 Kif1a Vps16 Elavl4 Tnks Fry Ift172 Sept9 Cetn2 Rabl6 Fer Pacsin3 Ubr4 Kalrn Cct5 Kif3a Clasp2 Myl4
Miscellaneous
Ap3m1 BC052040 Zfp385b Cmtm5 Arhgap23 Gnl1 Prrc2c Ttc7b Kiaa0195 Smap Tanc2 Gpr158 Dock11 Shisa7 Mast3 Scube1 Pmch Kiaa1239 Ppm1g Nemf Gprin3 Dmxl1 Dnajb11 Igsf9b Limch1 Nptx2

signaling proteins, consistent with the whole brain data (Fig 4*C*). Similarly, Hdac4 interactions with vesicle trafficking and neuronal function related proteins were also evident in the striatum. The largest number of known Htt-interacting proteins were also found in these protein classes, suggesting a possible functional relevance in HD for this enrichment. Also like the whole brain IPs, the Hdac5 interactome in dissected striatum (supplemental Fig. S7, supplemental Table S6) was again enriched for cytoplasmic proteins and distinct from the interactome of Hdac4. In addition to the 14–3-3 proteins, only three other proteins, Thbs1, Cat, and Fry, were shared between the observed Hdac4 and Hdac5 interactions, adding further support to the distinct role of Hdac4 in HD disease.

To gain further insights into the tissue type-enriched Hdac4 associations, we next compared the Hdac4 interactomes derived from whole brain and striatum. Approximately 23% of the interactions were shared, whereas ~34% were unique to the whole brain IP and ~43% were unique to the striatum IP (supplemental Fig. S8*A*). For Hdac5, this distribution was different in that ~55% of the filtered interactions were found in both whole brain and striatum, whereas only ~6% were unique to whole brain and ~39% unique to striatum (supplemental Fig. S8*B*). This suggests that Hdac5 may have a large subset of functions that are shared between the striatum and the rest of the brain (represented by >55% of its interactions). For both Hdacs, the interactions observed only in the whole brain and not in the striatum may derive from other brain regions. The relatively large number (>34%) of such Hdac4 interactions suggests that Hdac4 may have distinct functions in brains regions outside of the striatum, though this would need additional experimentation to confirm. Conversely, the interactions found only in striatum may be unique to this brain region or may pass the specificity filter because of the cleaner background and lower complexity of the striatum IPs. The percentages of interactions uniquely enriched in the striatum are similar for Hdac4 and Hdac5, suggesting that both enzymes have specific functions within this brain region. However, the classification of these interacting proteins according to their biological roles indicates that only Hdac4 has enriched associations with neuronal processes and vesicular trafficking proteins. Interestingly, the relative proportions of shared and unique interactions for Hdac4 and Hdac5 in whole brain and striatum remain largely the same when considering only the interactions specific in the Q20 (normal) conditions, indicating that the observed distribution of interactions is not dependent on Htt mutational status (supplemental Fig. S8*C*–S8*D*).

To examine the shared and differential functional classes in the Hdac4 interactomes further, we performed overrepresentation analyses of biological process gene ontologies using ClueGO in Cytoscape (Fig 5*A*). Most enriched classes showed an increased number of interactions present in the striatum, including the functional categories of synaptic organization, organelle localization, and cytoskeletal transport. A closer look at the regulation of synapse organization category (Fig 5*B*) revealed sub-categories involved in dendritic development. Additionally, an examination of the categories of establishment of organelle localization and regulation of receptor-mediated endocytosis (Fig 5*C*) revealed subcategories involved in vesicle trafficking driven by proteins enriched in the striatal IPs. Taken together, these results suggest that, in the striatum, Hdac4 may play a role in synaptic development and function and thus is poised to exacerbate synaptic decline in HD patients if Hdac4 becomes dysregulated during the disease.

Hdac4 Exhibits polyQ-dependent Enriched Interactions with the WASH Complex—As our striatum *versus* the whole brain comparison highlighted the enrichment of Hdac4 associations with vesicle trafficking and neuronal function related proteins, we further investigated the age- and Q length-dependent abundance trends for these associations (Fig 6*A*, left). Four groups were evident, with group 1 consisting of Inpp5j and Prex2 and exhibiting decreased Hdac4 association with age but increased association in the Q140 2 M old mice. The most significant changes ($p \leq 0.001$) were observed within group 3 (Fig 6*A*, right), which contained proteins that increased considerably in association with Hdac4 at both ages in Q140 mice. Within this group were members of the WASH complex, which we initially discovered in the whole brain Hdac4 IP. Providing further support for this Hdac4 association, in the striatum we found more complex components and accessory proteins, including Washc2, Washc5, and Snx27. The other complex components, Wash, Washc3, and Washc4 were also detected in the striatum IP, completing this pentameric complex, but these proteins were present at lower levels and therefore did not pass our stringent specificity cutoff (SAINT >0.95). However, it is noteworthy that all WASH components displayed the exact same changes in their associations with Hdac4 in response to polyQ length and age, showing a substantial increase in association in Q140 mice (Fig 6*B*). Therefore, the specific focus on this HD-affected tissue highlighted the increased Hdac4-WASH association in a disease condition.

FIG. 4. **The Hdac4 protein interaction network in the striatum of HD mouse models.** *A*, PCA of specificity-filtered Hdac4 interactions revealed Q length-dependent trends in the interactome. *B*, A Q-length dependent effect on overall Hdac4-interaction associations was observed in striatum. *** $p \leq 0.001$, Kruskal-Wallis test. *C*, Comparison of endogenous Hdac4 interactions in Q20 and Q140 mice at 2 and 10 months age. Each interacting protein is shown as a ring plot with the relative median MS1 abundance levels in each isolation condition depicted as indicated on the Hdac4 ring at the center of the network. Gene names shown in red are Hdac4 specific interactions that are also reported Htt interactions. Edges represent known protein-protein interactions and other associations present in the STRING database. Protein interactions have been functionally grouped and labeled in blue text. Interactions were truncated so that a specificity score of 0.97 was required for 10-month IPs for illustrative purposes. The additional interactions are provided in supplemental Fig. S5.

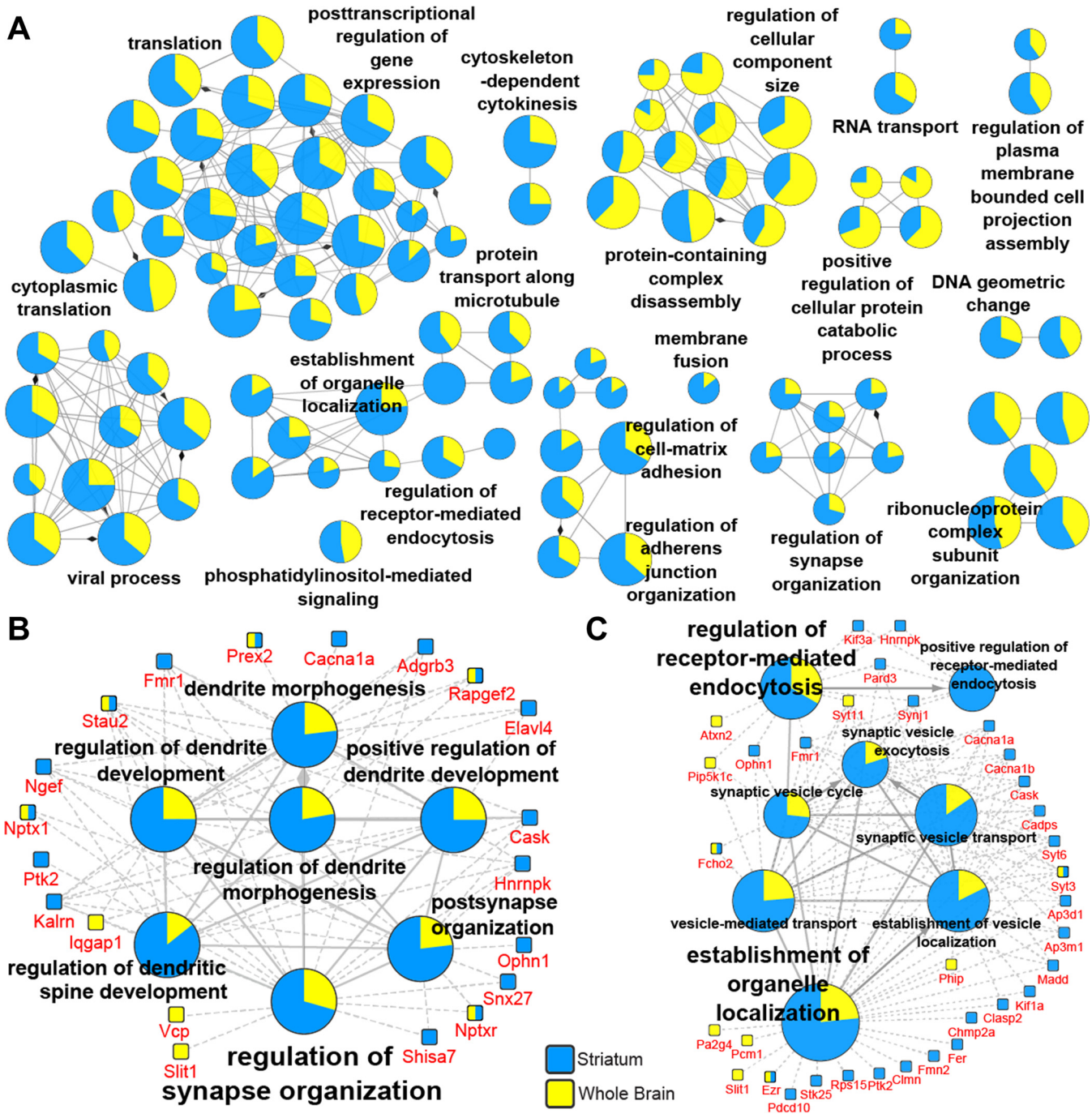

FIG. 5. **Comparison and characterization of Hdac4 interactomes in the whole brain and striatum.** *A*, Biological process gene ontology analysis of shared and unique Hdac4 interactions in whole brain and striatum. Blue represents interactions in striatum and yellow interactions in whole brain. Pie charts show relative proportion of interactions in each functional class that were present in whole brain or striatum. *B*, Examination of the regulation of synapse organization GO term shows an enrichment in striatal IPs of proteins involved in dendrite generation. *C*, Examination of receptor-mediated endocytosis and organelle localization GO terms shows an enrichment in striatal IPs of vesicle trafficking and synaptic proteins.

Given this pronounced polyQ-dependent enrichment for the WASH complex, we aimed to validate this previously unreported association of Hdac4. We first tested the few commercially-available antibodies against WASH complex members, but these did not work for immunoaffinity purifications of the baits. Therefore, we next undertook a systematic cloning approach to co-express GFP-tagged HDAC4 with individual FLAG-tagged components of the WASH complex. Our goals were to determine whether we could confirm the association, and whether we could determine with which

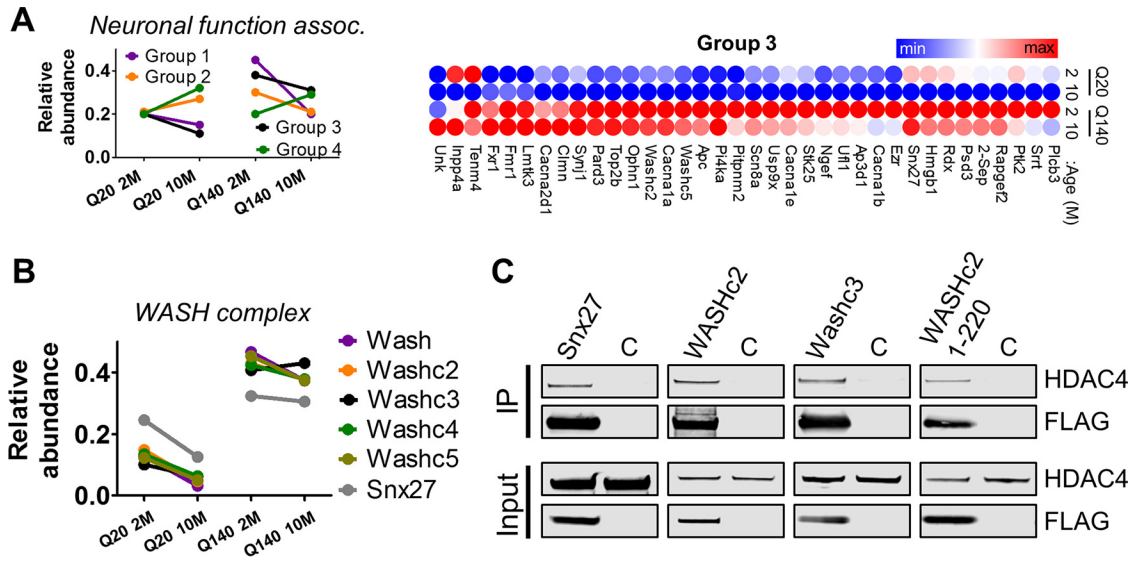

FIG. 6. **Hdac4 displays a polyQ-dependent enriched association with the Wiskott-Aldrich Syndrome Protein and SCAR Homolog (WASH) complex.** *A*, Line graphs of neuronal function associated proteins show differential patterns of Hdac4 association in striatum. The heatmap below depicts the relative changes in each protein across conditions for group3 of the neuronal function associated interactions with the minimal amount associated with Hdac4 getting a blue color and the maximal association with Hdac4 a red color. *B*, Components of the WASH complex present in striatum data set show concerted relative abundance changes in association with Hdac4 and an overall increased association in Q140 mice. *C*, Reciprocal IPs of FLAG-tagged WASH complex members in HEK-293T cells confirm association of the WASH complex with HDAC4.

member(s) of the complex HDAC4 most prominently interacts. For most WASH complex members (Wash1, Washc3 and Washc5), we were successful in performing cloning using mouse cDNA, except for WASHc2, which we had to amplify from human cDNA. We also cloned the accessory factor Snx27 from mouse cDNA. We then performed reciprocal isolations of the individual WASH members and investigated the co-isolation of HDAC4 from HEK-293T cells. Our results confirmed the association of HDAC4 with the WASH complex. Specifically, we observed the reciprocal isolation of HDAC4 with immunoenriched WASHc2, Washc3, and Snx27 (Fig. 6*C*). Wash1 and Washc5 did not show the reciprocal isolation of HDAC4 (supplemental Fig. S9); therefore, these proteins may associate with HDAC4 indirectly through the interactions of the other complex members.

We next investigated which domains may mediate this interaction between the WASH complex and HDAC4. We focused this study on WASHc2, as this was the most enriched WASH component in our Hdac4 IP-MS-derived interactomes and was the only component found to be specifically enriched in both the whole brain and the striatum. We noted that the first 220 amino acid region of WASHc2 has been shown to be enough to promote interaction with the other members of the WASH complex (47, 52). Therefore, we tested whether this region alone can co-purify HDAC4. Indeed, we observed that isolation of this N-terminal WASHc2 fragment also enriched HDAC4, suggesting that the interaction of HDAC4 with WASHc2 might be mediated by this region.

A Multiomics Perspective of Hdac4 Interactions: Integration with the HD Mouse Proteome and Transcriptome—Unlike our findings from the whole brain IP data set, in the striatum we see an increase in interaction abundance for most proteins in the Q140 condition (Fig 3*A versus* 4*B*). One possible explanation of increased interaction abundances is a corresponding increase in the overall proteome abundance of these proteins in the striatum of Q140 mice. To investigate this possibility, we took advantage of a proteomics data set publicly available from PRIDE (PXD006302) that contained label-free whole proteome analyses and RNAseq transcriptome analyses from (13). The new proteome data was generated in collaboration with the CHDI foundation as a resource to complement their proteome study at 6 months of age (13) but has not yet been utilized in a publication. Importantly, these multiomics experiments were performed on dissected striatum and included mice with the same Htt Q lengths and ages as our study.

For the proteome analyses, we reanalyzed the raw data using the same label-free quantification pipeline as our interaction data sets (supplemental Table S7). The processed RNAseq data in supplemental Table S1 from (13) and was used without further processing. We mapped the proteins that were quantified in at least half of the samples to their Entrez gene identifiers and then overlapped this with the transcriptome data. This resulted in a total of 7939 protein-mRNA pairs for further analysis (Fig 7*A*, supplemental Table S8).

To begin, we first examined the proteome in this combined data set for signature protein differences correlated with expanded polyQ length at both 2 and 10 months. We saw a clear separation of the Q140 and Q20 samples in PCA space (supplemental Fig. S10*A*) indicating that the polyQ expansion may

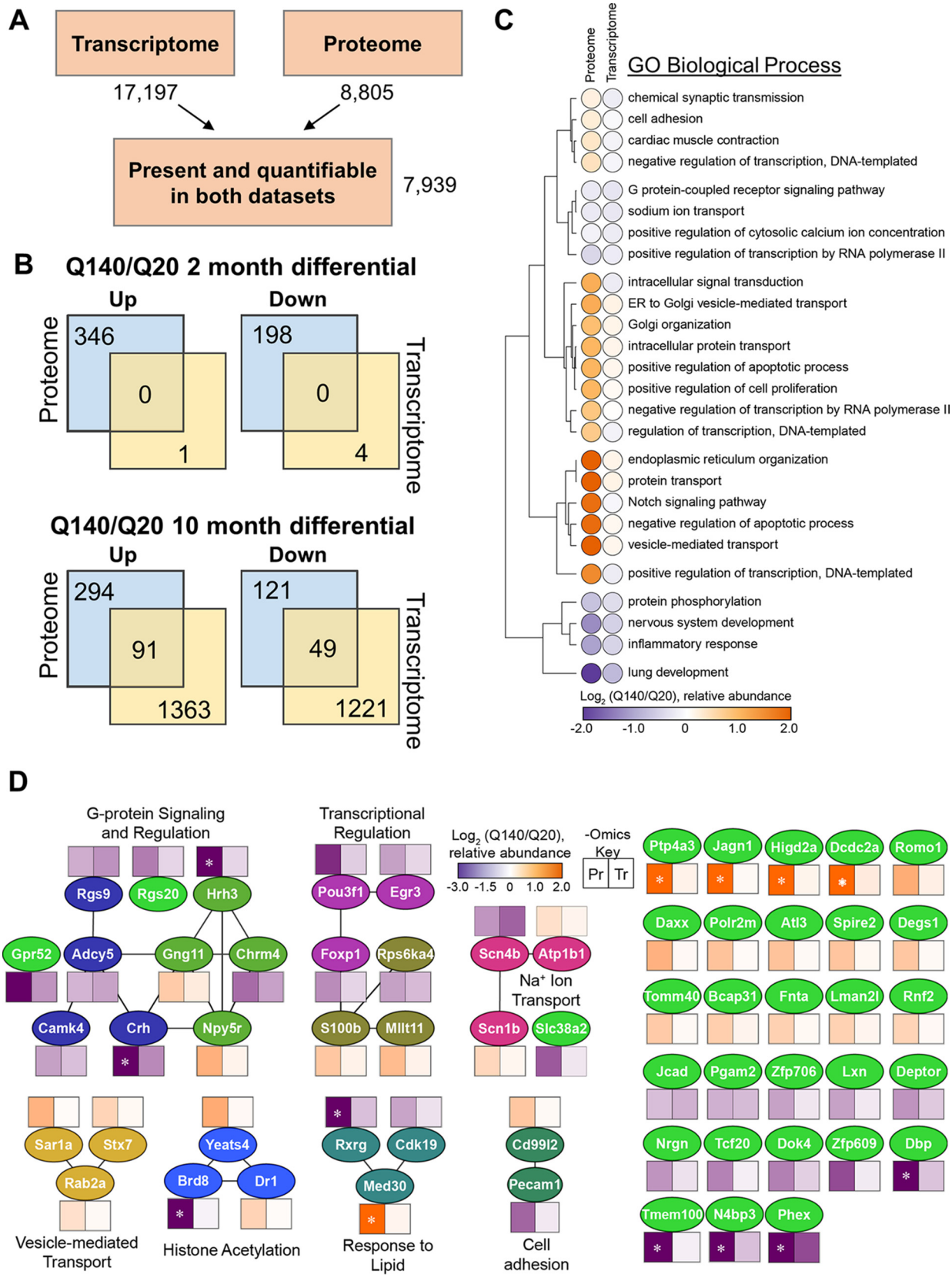
A
Transcriptome
Proteome
17,197
8,805
Present and quantifiable in both datasets
7,939
B
Q140/Q20 2 month differential
Up
Down
Proteome
Transcriptome
346
0
1
198
0
4
Q140/Q20 10 month differential
294
91
1363
121
49
1221
C
Proteome
Transcriptome
GO Biological Process
chemical synaptic transmission
cell adhesion
cardiac muscle contraction
negative regulation of transcription, DNA-templated
G protein-coupled receptor signaling pathway
sodium ion transport
positive regulation of cytosolic calcium ion concentration
positive regulation of transcription by RNA polymerase II
intracellular signal transduction
ER to Golgi vesicle-mediated transport
Golgi organization
intracellular protein transport
positive regulation of apoptotic process
positive regulation of cell proliferation
negative regulation of transcription by RNA polymerase II
regulation of transcription, DNA-templated
endoplasmic reticulum organization
protein transport
Notch signaling pathway
negative regulation of apoptotic process
vesicle-mediated transport
positive regulation of transcription, DNA-templated
protein phosphorylation
nervous system development
inflammatory response
lung development
Log2 (Q140/Q20), relative abundance
-2.0 -1.0 0 1.0 2.0
D
G-protein Signaling and Regulation
Rgs9
Rgs20
Hrh3
Gpr52
Adcy5
Gng11
Chrm4
Camk4
Crh
Npy5r
Transcriptional Regulation
Pou3f1
Egr3
Foxp1
Rps6ka4
S100b
Mllt11
Log2 (Q140/Q20), relative abundance
-3.0 -1.5 0 1.0 2.0
-Omics Key
Pr
Tr
Scn4b
Atp1b1
Na+ Ion Transport
Scn1b
Slc38a2
Ptp4a3
Jagn1
Higd2a
Dcdc2a
Romo1
Daxx
Polr2m
Atl3
Spire2
Degs1
Tomm40
Bcap31
Fnta
Lman2l
Rnf2
Jcad
Pgam2
Zfp706
Lxn
Deptor
Nrgn
Tcf20
Dok4
Zfp609
Dbp
Tmem100
N4bp3
Phex
Sar1a
Stx7
Rab2a
Vesicle-mediated Transport
Yeats4
Brd8
Dr1
Histone Acetylation
Rxrg
Cdk19
Med30
Response to Lipid
Cd99l2
Pecam1
Cell adhesion

be driving proteome level differences. We also noted that the 2- and 10-month-old mice were more separated in PCA space in the Q140 mice than the Q20 mice, indicating that advanced age can further enhance the proteome alterations observed during HD. To examine the age and Q-dependent proteome changes in these mice, we compared proteins that were significantly up and down regulated at each age in Q140 mice compared with Q20 mice (supplemental Fig. S10*B*). We chose an adjusted p value cutoff of ≤ 0.1 for this analysis to make it comparable with the previous published analysis at 6 months (13). We next analyzed the proteins with increased abundance in Q140 mice at both ages (supplemental Fig. S10*B*, *left*) using the ClueGO Cytoscape app to perform a combined Gene Ontology (GO) Biological Process and Reactome pathway enrichment analysis (supplemental Fig. S10*C*). A subset of proteins was enriched in ion transmembrane transport and synaptic vesicle transport pathways at roughly equal proportions in both ages. Additionally, we found neurotransmission and mitochondrial related functions to be up-regulated in both ages, but more so at 10 months. Finally, we noted a single enriched category (positive regulation of myelination) that was more enriched in the 2-month-old mice. All these categories are related to energy generation and synaptic functions, which are known to be dysregulated in HD (53, 54). Interestingly, the proteins with significantly decreased abundance in Q140 mice were not as functionally clustered as the up-regulated proteins. Enrichment analysis yielded only sparse results related to mitochondrial membrane organization because of an insufficient number of differential proteins with the same ontology.

We next asked whether the observed proteome differences are also present at the transcript level in these mice using the same significance cutoff in both data sets (adjusted p value ≤ 0.1). In the 2-month-old mice, almost no significantly differential transcripts were present, but in the 10-month-old mice, we observed a subset of genes that exhibited concerted significant differences at both protein and transcript level (Fig 7*B*). To investigate these concerted differential genes in the 10-month samples, we examined them in the context of a set of previously defined mRNA modules (13) that were found to have a polyQ-dependent variation across three ages (2, 6, and 10 months) in the striatum. We found that of the 140 concerted differential genes in Fig 7*B*, 101 (72%) fell into 6 of the 37 mRNA modules defined by the Langfelder *et al.* study (13) (supplemental Fig. S11). The largest proportion of differential genes fell into module 2, which was enriched for striatal marker genes and was negatively correlated with polyQ length (13). Other genes fell into modules positively correlated with polyQ length that were enriched for mitochondria (Modules 9 and 43) and p53 signaling and cell division (Module 20) (supplemental Fig. S11). In all, this analysis demonstrated that at least some of the polyQ-dependent transcriptional changes observed in relevant functional categories were also preserved at the proteome level in symptomatic Q140 mice.

We next investigated whether there are functional correlations between gene-protein pairs that exhibited concerted abundance changes outside of the previously defined functional mRNA modules. Ontologies for each gene were obtained from UniProt, and the average relative gene and protein abundances (Q140/Q20) were calculated for each ontology based on the respective annotated genes ($N \geq 3$). The gene ontologies were visualized by hierarchical clustering as a functional of average relative abundances (Fig 7*C*, supplemental Fig. S12*A*–S12*B*). These analyses revealed that genes involved in ion transport, G protein-coupled receptor signaling, and nervous system development had concerted decreases. We also observed concerted increases in genes involved in vesicular trafficking, protein transport, and respiratory electron transport.

Examination of the annotated functional connectivity of the concerted gene-protein pairs identified several small interconnected networks, most prominently for G-protein signaling and transcriptional regulation (Fig 7*D*). For instance, one of the gene-protein pairs with the greatest down-regulation in the Q140 proteome was Gpr52. Gpr52 is an orphan striatal-enriched G protein-coupled receptor that was previously shown to modulate Htt (55). Moreover, knockout of Gpr52 in HD mouse models lowered mutant Htt and rescued pathological HD phenotypes, whereas a Gpr52 antagonist decreased soluble mutant Htt levels (56). This G protein network also included down-regulated corticotropin-releasing hormone (Crh), which was previously reported to be decreased in the basal ganglia of post-mortem HD brains (57). Given an increasing appreciation that transcription dysregulation (transcriptionally and epigenetically) is a prominent facet of HD pathogenesis (58), our identification of a dysregulated transcriptional network containing the forkhead box protein p1 transcription factor (Foxp1), and a three-member network involving histone acetylation activity is noteworthy. Foxp1 has striatal selective expression and likely serves a neuroprotective role in HD (59). The cluster of proteins involved in histone acetylation (Yeats4, Brd8, and Dr1) can be members of the NuA4 and ATAC histone acetyltransferase (HAT) complexes (60, 61). Yeats4/Gas41 and Brd8 are known to function within

FIG. 7. **Multiomic analysis of striata from HD model mice.** *A*, Integration of proteome and transcriptome from HD model mice resulted in 7939 quantifiable protein-mRNA pairs for analysis. *B*, Venn diagrams of significantly differential (adjusted $p \leq 0.1$) proteins and transcripts show both concerted and non-concerted changes in gene expression. *C*, Functional analysis of genes with concerted protein and RNA changes revealed co-regulated processes. *D*, STRING functional interaction network of individual co-regulated transcripts/proteins at 10 months of age that were annotated to the GO Biological Processes from (*C*). Nodes were color-coded and grouped by k-means clustering, labeled with respective genes and heatmaps (squares) of the relative abundances (Q140/Q20) for the Proteome (Pr) and Transcriptome (Tr). *, represents proteins that were uniquely detected in either Q140 or Q20 10 month proteome.

NuA4 HAT complexes as acetyllysine readers (62, 63), whereas Dr1/NC2β is a member of the ATAC complex with HAT and nucleosome remodeling activities, the latter of which likely involves the histone fold domain of Dr1 (61).

Despite an overall correlation between RNA and protein abundance of ~0.45 (supplemental Fig. S12*C*), which is similar to what has been previously reported for other high throughput RNA-protein studies (13, 64, 65), we observed only a small number of genes to exhibit a significant shift in abundance in the same direction. Therefore, we asked whether a better concordance between differential functional categories was present. To do this, we individually took the proteins and mRNA transcripts that were significantly higher in Q140 striata at 10 months (bottom left Venn diagram, Fig 7*B*) and performed GO biological process enrichment analysis. Comparison of the significantly enriched GO terms showed that 71% of the GO terms associated with the differential proteins were also present in the transcriptome (supplemental Fig. S12*D*). This suggested that, although most individual genes may not be regulated at both the transcript and protein level, the overall pathways and functional gene groups may be regulated in a concerted fashion. Further examination of the shared GO terms showed enrichments primarily in mitochondrial-related processes, including mitochondrial organization, metabolism, electron chain transport, and nitrogen compound transport (supplemental Fig. S13). The GO terms associated only with proteome alterations were mostly assigned to categories related to neuronal function, including ion, transmembrane, and neurotransmitter transport, as well as to learning or memory (supplemental Fig. S14). On the other hand, the transcriptome specific enrichments were primarily related to metabolism, Golgi vesicle transport, and mitochondrial membrane organization (supplemental Fig. S15). The exact same comparison could not be made for the proteins and transcripts that were significantly decreased in the Q140 10-month mice as the decreased proteins were not enriched for any GO biological process terms, likely because of the small number of differential proteins. The transcriptome for the 10-month mice was downregulated for genes involved in synaptic transmission, protein phosphorylation, and regulation of ion transport (supplemental Fig. S16).

Of interest, a subset of enriched GO terms highlighted by this multiomic analysis were related to our Hdac4 interactome, notably the vesicle trafficking and synaptic function related categories. Therefore, we next asked whether the Hdac4 interactions identified in our striatum IP were observed to have altered abundances in either the proteome or transcriptome data sets (Fig 8*A*). We noted that 73 interacting proteins had significantly differential transcripts, but only 15 had significantly differential proteins levels. Among these proteins, only Stag1 was found significantly down-regulated at both the protein and transcript level in the 10-month mice (Fig 8*B*). Because there was only one Hdac4 interacting protein with concerted changes at the proteome and transcriptome level, we decided to compare Q-dependent fold changes at each age and cluster them by Euclidean distance to look for patterns that could be significant but at sub-threshold levels. No overt conserved patterns were observed between the three data sets (Fig 8*C*). However, individual protein interactions did show differential trends in ratios across the interactome and proteome or transcriptome, with the proteome demonstrating the most pronounced effect.

To investigate this further, we normalized all interactions by the proteome abundances to determine if even non-significant changes in proteome abundances would result in overt thematic changes in functional sub-groups of the Hdac4 interactome (supplemental Table S9). The proteins with the most pronounced changes were further examined in a heatmap, ordered from highest to lowest association with Hdac4 in the 10-month samples, as adjusted by the proteome (Fig 8*D*). The members of the WASH complex did not have prominent changes in their abundance at the proteome level, indicating that the observed increase in their association with Hdac4 in the striatum of Q140 mice in our IP data set is not driven by a chance in their overall protein abundance, but rather by another regulatory event. It is noteworthy that even for those proteins that did exhibit some proteome abundance changes, the proteome-corrected associations with Hdac4 in the IP data set largely followed the original trends. This highlights that the identified changes in Hdac4 interactions are more likely functionally-driven rather than simply abundance-driven, emphasizing the value of examining interaction studies from multiple omic perspectives.

DISCUSSION

Our multiomic study of Hdac4 highlights the unique role that this protein performs in neuronal tissues, as compared with its previously known functions in human cell culture (28). In HD mouse brain, we see enrichments for proteins involved in RNA binding, vesicle trafficking, synaptic function, and other related neuronal functions. By comparing interactomes generated from both whole brain and a single brain region, we were able to identify Hdac4 interactions that are enriched in the striatum, giving us clues into region-specific Hdac4 roles. Performing our interactome analysis in four different conditions, non-disease and disease polyQ lengths at pre- and post-symptomatic ages, further allowed us to identify sets of functionally related proteins that have altered associations with Hdac4 in response to age or disease progression. Finally, the integration of whole proteome and transcriptome data sets from these HD mouse models offered a perspective of the impact of mutant Htt and age on protein abundance and gene expression patterns, and how these synergize with functional enrichments observed in our Hdac4 interactomes. Below we discuss some of the main findings from this multiomic study.

We observed a strong enrichment in cytoplasmic Hdac4 protein interactions, in conjunction with increased phosphor-

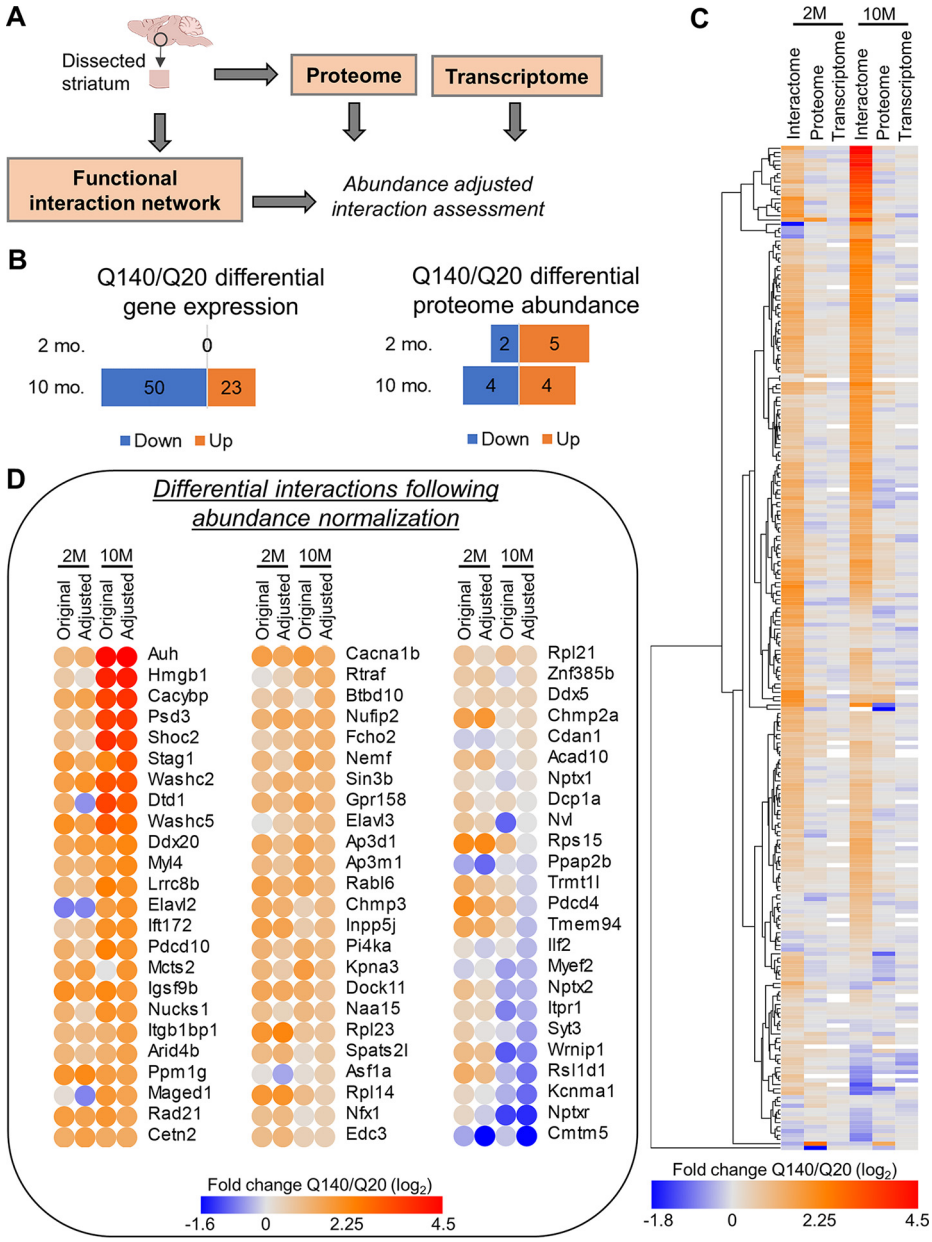

FIG. 8. **Integration of the Hdac4 interactome with proteome and transcriptome alterations in HD.** *A*, Workflow of data sets utilized to generate multiomics-informed data set. *B*, Number of significantly increased and decreased proteins and transcripts in the omics data sets. *C*, Heatmap of Q140/Q20 fold changes at 2 and 10 months of age in interactome, proteome, and trancriptome. *D*, Heatmap of most changed Hdac4 interactions following background proteome abundance correction. Original and adjusted values are shown.

ylation levels (in brain when compared with cultured T-cells) on a residue important for Hdac4 cytoplasmic shuttling. These findings support previous reports of predominant cytoplasmic Hdac4 localization in the mouse brain and proposed cytoplasmic function in HD mouse models (23). Our identification of proteins involved in vesicle trafficking, synaptic function, and cytoskeletal regulation (Fig 2*A*) offers hypotheses for the mechanisms underlying the previously observed rescue of synaptic function in HD mice on Hdac4 knockdown. A possible interpretation is that Hdac4 may regulate synaptic vesicle trafficking or neurotransmitter recycling and that this function becomes disrupted in HD. In support of this hypothesis, another study observed neurons with synaptic localization of Hdac4 (27), indicating that this may be a normal function for Hdac4. However, it is also possible that these interactions represent the active trafficking of Hdac4 to different subcellular regions, and that this proper trafficking is disrupted by aggregated Htt, resulting in Hdac4 mis-localization or possibly accumulation at the synapse, with subsequent disruption of synaptic function. It should be taken into account that, as only one antibody was found to be suitable for IP-MS experiments for each Hdac, we cannot rule out the possibility that

a subset of the proteins that passed the specificity filtering may be derived from possible antibody cross-reactivity rather than by association with Hdac4 or Hdac5. We hope that the protein interactions identified in our study, particularly those that functionally correlate with the perturbations identified in the multiomic data, provide a set of potential targets that will aid future studies aimed at elucidating the roles of Hdac4 at the synapse.

Additional support for an Hdac4 role in vesicle trafficking and synaptic function was provided by our interactome study in dissected striata (Fig 4*C*), which demonstrated strong enrichment in proteins involved in these functional categories (Fig 5*A*). The enrichment in synapse organization included proteins like Snx27, a known binding partner of the WASH complex that we also found in the Hdac4 interaction network. The WASH complex is an actin-regulating multiprotein complex involved in endosomal sorting and trafficking. Of note, the WASH complex and its associated binding proteins have been previously implicated in two other neurological disorders, Parkinson's Disease (66) and hereditary spastic paraplegia (67). In our study, we observed a clear concerted pattern of association with Hdac4 for all members of the WASH complex, in which the Q140 mice had a significantly higher level of complex components associated with Hdac4. We further confirmed this association of Hdac4 and the WASH complex by reciprocal isolations of HDAC4 by several members of the WASH complex (WASHc2 and Washc3, and the accessory factor Snx27). Of note, a recent study found that association of Snx27, the WASH complex, and retromer facilitated the recycling of endosomal cargos to the plasma membrane (68). It is tempting to speculate that this increased Hdac4-WASH association could play a role in the synaptic dysregulation in HD, and this would require further investigation.

Along with the increased Hdac4-WASH complex association, we noted a general trend of elevated interactions in the Q140 mice (Fig 4*B*). Among these interactions were those with cation channel complex proteins, particularly the N-type calcium channel proteins. Some of these, Cacna1a and Cacna1b, were also present in the synaptic vesicle transport GO term that was enriched in the striatal interactome (Fig 5*C*). This family of proteins is of interest in this context, having been previously implicated in HD, though only Cacna2d1 was reported as an Htt-interacting protein. Previous work has shown that mutant Htt can cause alterations to the cell surface expression of Cacna1b and disrupt its interactions with regulatory proteins (69). Although we do not have cell surface measurements of Cacna1b abundance, we did note a slight increase in protein abundance in our proteome data set. The association of Hdac4 with these calcium channel proteins provides additional evidence that Hdac4 has a role in synaptic function in HD.

In addition to Cacna2d1, we observed several previously reported Htt-interacting proteins in our Hdac4 interactomes. This suggests that, although we did not detect Htt in our Hdac4 interactomes, a possible indirect interaction (either physical or functional) between Htt and Hdac4 may exist. Interestingly, the Htt-interacting proteins that also associated with Hdac4 was increased in the Q140 10-month-old condition (supplemental Fig. S8*E*–S8*F*). This was not observed for Hdac5, adding additional weight to the possibility of a functional Hdac4 association with Htt via these common interacting proteins.

The Hdac5 interaction networks were substantially distinct from Hdac4, with only the 14–3-3 proteins and five other proteins present in both interactomes and no major Q-length dependence in the interaction levels observed. Hdac5 also appears to be primarily cytoplasmic in the brain and associated prominently with tubulin and the centrosome. The almost completely unique set of interactions for Hdac4 and Hdac5 in the brain does not mirror observations from human cell culture experiments with T cells and HEK293 cells, where overlapping interactions were detected, though these were primarily nuclear associations (28). Other than the 14–3-3 proteins, only Catalase (Cat) and Protein furry homolog (Fry) were consistent among all of the interactomes generated. Fry may act as a scaffold protein to bridge Polo-like kinase 1 and Aurora kinase A, and aurora kinases have been shown to phosphorylate class IIa Hdacs in cells (49), thus it is possible that a similar regulation occurs in this biological system.

A primary goal of HD research is to identify those proteins that are mostly directly involved in conveying the cellular pathology of mutant Htt. Omics studies have the potential to significantly contribute to this goal. Yet the inherent nature of these approaches to provide large, unbiased data sets can present challenges for data summarization and interpretation. Although targeted omics investigations, such as subcellular proteomes or interactomes are powerful, as illustrated by our protein network analyses of Hdac4 interactions in the striatum (see Fig 4C), the functional assessment of putative interactions still covers a reasonable proteome space across diverse biological processes. Therefore, additional reductionist strategies are required to maximize biological insights. The integration of multi-omics data sets has the potential to provide these insights and expedite the design of tractable, hypothesis-testing studies. In the current study, we viewed our Hdac4 interactions from the perspective of proteomes and transcriptomes perturbed by HD to identify common feature sets at the pathway and gene level. Though not yet fully published, dual omic data sets for the same HD mouse models at 2 and 10 months of age were available in public repositories. This also highlights the value of making omic data sets available to the scientific community for re-analysis from different biological perspectives. We performed re-processing of the raw quantitative proteomics data to allow for equivalent comparison to our interactome data set. Pathway and biological process enrichment analyses on differential genes identified with

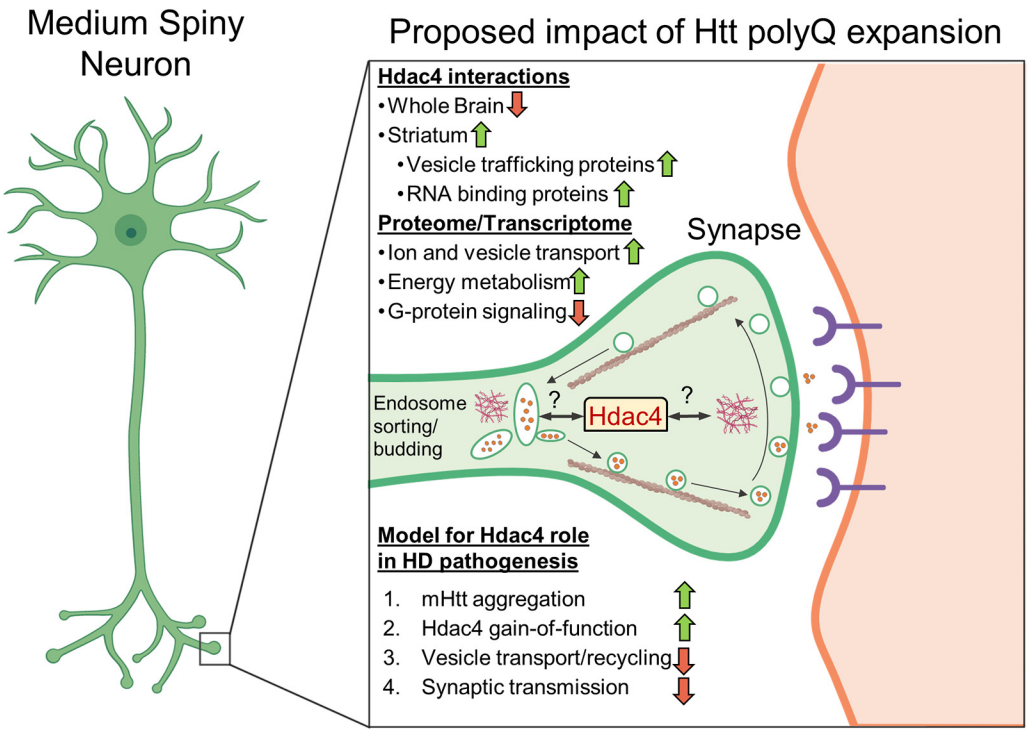

FIG. 9. **Potential model of role for Hdac4 in Huntington's Disease.** Our observations in this study identified Hdac4 associations with RNA binding proteins, proteins involved in vesicle trafficking, as well as various proteins involved in synapse function. Integrating these observations with our multiomic analysis and known hallmarks of HD pathogenesis suggests a model whereby mHtt aggregation leads to an average striatum-specific increase in Hdac4 interactions, potentially representing gain-of-function effect that together results in defects in vesicle transport/recycling and decreased synaptic transmission.

concerted changes at the proteome and transcriptome level identified key enriched processes that were also over-represented in the striatal interactome (Fig 4*C versus* 7*C*), most notably processes associated with synaptic functions such as vesicle trafficking and recycling and synaptic transmission. However, it is also interesting to consider why there are nearly as many proteome changes in the younger mice as the old despite almost no difference in the transcriptome at 2 months of age. HD has been shown to have both proteostatic and transcriptional dysfunctions, and it is possible that the proteostatic/translational differences are more apparent in the younger mice and the transcriptional effects are detected at more advanced age. Indeed, the transcriptome analysis by Langfelder *et al.*, which examined striatum, cortex, and liver at three different ages, showed almost no HD-dependent transcriptional differences at the 2-month time point (13). However, the authors observed that by 6 months of age, all tissues had detectable levels of transcriptional dysregulation. The Langfelder study also showed that the 6-month age striatum had more differentially regulated transcripts than the 10-month-old mice, further highlighting the temporal nature of this dysregulation. Altogether, these previous reports and our current study show the need for integrating multiomic data sets for understanding the contribution of complex biological processes to disease phenotypes.

Another interesting result from our Hdac4 striatal interactome that we further refined using multi-omics comparisons was the observation of polyQ-dependent increases in the protein interaction levels. As discussed above, this was not observed for proteins associating with Hdac5, which suggested that many of the Hdac4 interactions are uniquely regulated in HD. Yet, the possibility existed that differential regulation at the transcriptome and proteome levels could influence these Hdac4 interaction changes. Our integration of the transcriptome, proteome, and Hdac4 interactome abundances strongly suggest that the polyQ-dependent modulation of interactions occurs largely at the post-translational level. For most interacting proteins, their proteome abundance levels were relatively unchanged. An exception to this was the cohesin subunit SA-1 (Stag1), which showed opposing omic abundance changes. Stag1 exhibited a 2-fold increase in association with Hdac4, whereas its overall abundance within the proteome was decreased by 2-fold, suggesting that the potentiation of this interaction is precisely modulated. The interaction could be potentiated within specific cellular compartments, or given our model system, in specific cell types. Functionally, Stag1 is a member of the cohesion complex, which is well-known for its role in chromosome structure maintenance during the cell cycle (70), but also for its role in regulating gene expression (71), the latter of which would be relevant for post-mitotic cells. In-

deed, CNS and limb developmental defects are observed when cohesin functions are disrupted, such as in individuals with Cornelia de Lange syndrome (72). Moreover, in mouse models, low cohesin expression caused abnormal dendrite and synapse formation (73). Although the proteome analyses did not detect polyQ-dependent changes in other members of the cohesin complex, several cohesin complex members contain a HEAT domain as does Htt (74). Given there is currently no known functional link between Stag1, or the cohesin complex, and HD pathogenesis, understanding the functional significance of the Hdac4-Stag1 will require further investigation.

Overall, our observation that polyQ-dependent effects on Hdac4 interaction abundances are largely independent of their respective proteome changes suggests that the primary influence of mutant Htt on Hdac4 is to alter the composition and/or stability of its associated proteins. This could be achieved through several mechanisms, including changes in post-translational modifications (PTMs) or conformation, as well as protein sequestration. For example, as exemplified by class IIa Hdacs, phosphorylation status largely determines nuclear *versus* cytoplasmic localization (25), which subsequently impacts the composition of its interactions (75). In HD mouse models, Hdac4 remains cytoplasmic (23), though whether re-localization occurs within cytoplasmic compartments, such as at pre- or post-synaptic densities, remains a possibility. It is also possible that the PTM status of Hdac interacting partners are altered in the Q140 mice, potentiating their interaction with Hdac4. Although the broad impact of mutant Htt on the phosphoproteome is not known, Htt phosphorylation does play a critical role in modulating its aggregation and neuronal toxicity (76–78). For Hdac4 interactions that are decreased under conditions of Q140 Htt, mutant Htt may directly or indirectly sequester the interaction, preventing their normal cellular function(s). However, given the majority of Hdac4 interactions are potentiated and that Hdac4 reduction ameliorates HD phenotypes, a more likely hypothesis involves Hdac4 interactions acting as gain-of-function Htt toxicity modifiers (Fig. 9).

In all, the data presented here represents the first unbiased assessment of Hdac4 and Hdac5 interactions in mouse brain and highlights the potential for a specialized role of Hdac4 in the striatum. Our integrated multiomic assessment of Hdac4 interactions, protein abundance changes, and transcriptome changes in HD mouse models provides a comprehensive and contextualized view of the role Hdac4 is performing in HD and provides a resource for future investigation into the molecular mechanisms underlying these functions.

Acknowledgments—We thank Thomas Vogt, Ravi Iyer, Daniel Lavery, Kevin Silvester, Jeff Aaronson, and Esteban Chen at CHDI for helpful discussion.

DATA AVAILABILITY

The mass spectrometry proteomics data have been deposited to the ProteomeXchange Consortium via the PRIDE (79) partner repository with the data set identifier PXD011845.

* This work was supported by a grant from the CHDI Foundation to IMC. The CHDI Foundation is a not-for-profit biomedical research organization dedicated to Huntington's disease research and the development of therapeutics for treatment of this disease. CHDI participated in study design and data collection.

Ⓢ This article contains supplemental material.

§ To whom correspondence should be addressed: 210 Lewis Thomas Laboratory, Department of Molecular Biology, Princeton University, Princeton, NJ 08544. Tel.: 6092589417; Fax: 6092584575; E-mail: icristea@princeton.edu.

Author contributions: J.D.F., T.M.G., and I.M.C. designed research; J.D.F. and K.K.L. performed research; J.D.F., T.M.G., and I.M.C. analyzed data; J.D.F., T.M.G., and I.M.C. wrote the paper.

REFERENCES

1. Evans, S. J., Douglas, I., Rawlins, M. D., Wexler, N. S., Tabrizi, S. J., and Smeeth, L. (2013) Prevalence of adult Huntington's disease in the UK based on diagnoses recorded in general practice records. *J. Neurol. Neurosurg. Psychiatry* **84,** 1156–1160
2. Bates, G. P., Dorsey, R., Gusella, J. F., Hayden, M. R., Kay, C., Leavitt, B. R., Nance, M., Ross, C. A., Scahill, R. I., Wetzel, R., Wild, E. J., and Tabrizi, S. J. (2015) Huntington disease. *Nat. Rev. Dis. Primers* **1,** 15005
3. Waldvogel, H. J., Kim, E. H., Tippett, L. J., Vonsattel, J. P., and Faull, R. L. (2015) The Neuropathology of Huntington's Disease. *Curr. Top. Behav. Neurosci.* **22,** 33–80
4. (1993) A novel gene containing a trinucleotide repeat that is expanded and unstable on Huntington's disease chromosomes. The Huntington's Disease Collaborative Research Group. *Cell* **72,** 971–983
5. Ross, C. A., and Tabrizi, S. J. (2011) Huntington's disease: from molecular pathogenesis to clinical treatment. *Lancet Neurol.* **10,** 83–98
6. DiFiglia, M., Sapp, E., Chase, K. O., Davies, S. W., Bates, G. P., Vonsattel, J. P., and Aronin, N. (1997) Aggregation of huntingtin in neuronal intranuclear inclusions and dystrophic neurites in brain. *Science* **277,** 1990–1993
7. Kim, Y. E., Hosp, F., Frottin, F., Ge, H., Mann, M., Hayer-Hartl, M., and Hartl, F. U. (2016) Soluble oligomers of PolyQ-expanded Huntingtin target a multiplicity of key cellular factors. *Mol. Cell* **63,** 951–964
8. Scherzinger, E., Sittler, A., Schweiger, K., Heiser, V., Lurz, R., Hasenbank, R., Bates, G. P., Lehrach, H., and Wanker, E. E. (1999) Self-assembly of polyglutamine-containing huntingtin fragments into amyloid-like fibrils: implications for Huntington's disease pathology. *Proc. Natl. Acad. Sci. U.S.A.* **96,** 4604–4609
9. Kieburtz, K., MacDonald, M., Shih, C., Feigin, A., Steinberg, K., Bordwell, K., Zimmerman, C., Srinidhi, J., Sotack, J., Gusella, J., and et al. (1994) Trinucleotide repeat length and progression of illness in Huntington's disease. *J. Med. Genet.* **31,** 872–874
10. Mehta, S. R., Tom, C. M., Wang, Y., Bresee, C., Rushton, D., Mathkar, P. P., Tang, J., and Mattis, V. B. (2018) Human Huntington's Disease iPSC-derived cortical neurons display altered transcriptomics, morphology, and maturation. *Cell Rep.* **25,** 1081–1096.e6
11. Lin, L., Park, J. W., Ramachandran, S., Zhang, Y., Tseng, Y. T., Shen, S., Waldvogel, H. J., Curtis, M. A., Faull, R. L., Troncoso, J. C., Pletnikova, O., Ross, C. A., Davidson, B. L., and Xing, Y. (2016) Transcriptome sequencing reveals aberrant alternative splicing in Huntington's disease. *Hum. Mol. Genet.* **25,** 3454–3466
12. Labadorf, A., Hoss, A. G., Lagomarsino, V., Latourelle, J. C., Hadzi, T. C., Bregu, J., MacDonald, M. E., Gusella, J. F., Chen, J. F., Akbarian, S., Weng, Z., and Myers, R. H. (2015) RNA sequence analysis of human Huntington disease brain reveals an extensive increase in inflammatory and developmental gene expression. *PLoS ONE* 10, e0143563
13. Langfelder, P., Cantle, J. P., Chatzopoulou, D., Wang, N., Gao, F., Al-Ramahi, I., Lu, X. H., Ramos, E. M., El-Zein, K., Zhao, Y., Deverasetty, S., Tebbe, A., Schaab, C., Lavery, D. J., Howland, D., Kwak, S.,

Botas, J., Aaronson, J. S., Rosinski, J., Coppola, G., Horvath, S., and Yang, X. W. (2016) Integrated genomics and proteomics define huntingtin CAG length-dependent networks in mice. *Nat. Neurosci.* **19,** 623–633

14. Hu, H., McCaw, E. A., Hebb, A. L., Gomez, G. T., and Denovan-Wright, E. M. (2004) Mutant huntingtin affects the rate of transcription of striatum-specific isoforms of phosphodiesterase 10A. *Eur. J. Neurosci.* **20,** 3351–3363
15. McCaw, E. A., Hu, H., Gomez, G. T., Hebb, A. L., Kelly, M. E., and Denovan-Wright, E. M. (2004) Structure, expression and regulation of the cannabinoid receptor gene (CB1) in Huntington's disease transgenic mice. *Eur. J. Biochem.* **271,** 4909–4920
16. Cui, L., Jeong, H., Borovecki, F., Parkhurst, C. N., Tanese, N., and Krainc, D. (2006) Transcriptional repression of PGC-1alpha by mutant huntingtin leads to mitochondrial dysfunction and neurodegeneration. *Cell* **127,** 59–69
17. Hervas-Corpion, I., Guiretti, D., Alcaraz-Iborra, M., Olivares, R., Campos-Caro, A., Barco, A., and Valor, L. M. (2018) Early alteration of epigenetic-related transcription in Huntington's disease mouse models. *Sci. Rep* **8,** 9925
18. Steffan, J. S., Kazantsev, A., Spasic-Boskovic, O., Greenwald, M., Zhu, Y. Z., Gohler, H., Wanker, E. E., Bates, G. P., Housman, D. E., and Thompson, L. M. (2000) The Huntington's disease protein interacts with p53 and CREB-binding protein and represses transcription. *Proc. Natl. Acad. Sci. U.S.A.* **97,** 6763–6768
19. Boutell, J. M., Thomas, P., Neal, J. W., Weston, V. J., Duce, J., Harper, P. S., and Jones, A. L. (1999) Aberrant interactions of transcriptional repressor proteins with the Huntington's disease gene product, huntingtin. *Hum. Mol. Genet.* **8,** 1647–1655
20. Sharma, S., and Taliyan, R. (2015) Transcriptional dysregulation in Huntington's disease: The role of histone deacetylases. *Pharmacol. Res.* **100,** 157–169
21. Mielcarek, M., Benn, C. L., Franklin, S. A., Smith, D. L., Woodman, B., Marks, P. A., and Bates, G. P. (2011) SAHA decreases HDAC 2 and 4 levels in vivo and improves molecular phenotypes in the R6/2 mouse model of Huntington's disease. *PLoS ONE* **6,** e27746
22. Haberland, M., Montgomery, R. L., and Olson, E. N. (2009) The many roles of histone deacetylases in development and physiology: implications for disease and therapy. *Nat. Rev. Genet.* **10,** 32–42
23. Mielcarek, M., Landles, C., Weiss, A., Bradaia, A., Seredenina, T., Inuabasi, L., Osborne, G. F., Wadel, K., Touller, C., Butler, R., Robertson, J., Franklin, S. A., Smith, D. L., Park, L., Marks, P. A., Wanker, E. E., Olson, E. N., Luthi-Carter, R., van der Putten, H., Beaumont, V., and Bates, G. P. (2013) HDAC4 reduction: a novel therapeutic strategy to target cytoplasmic huntingtin and ameliorate neurodegeneration. *PLos Biol.* **11,** e1001717
24. Butler, R., and Bates, G. P. (2006) Histone deacetylase inhibitors as therapeutics for polyglutamine disorders. *Nat. Rev. Neurosci.* **7,** 784–796
25. Chawla, S., Vanhoutte, P., Arnold, F. J., Huang, C. L., and Bading, H. (2003) Neuronal activity-dependent nucleocytoplasmic shuttling of HDAC4 and HDAC5. *J. Neurochem.* **85,** 151–159
26. Verdin, E., Dequiedt, F., and Kasler, H. G. (2003) Class II histone deacetylases: versatile regulators. *Trends Genet.* **19,** 286–293
27. Darcy, M. J., Calvin, K., Cavnar, K., and Ouimet, C. C. (2010) Regional and subcellular distribution of HDAC4 in mouse brain. *J. Comp. Neurol.* **518,** 722–740
28. Joshi, P., Greco, T. M., Guise, A. J., Luo, Y., Yu, F., Nesvizhskii, A. I., and Cristea, I. M. (2013) The functional interactome landscape of the human histone deacetylase family. *Mol. Syst. Biol.* **9,** 672
29. Manza, L. L., Stamer, S. L., Ham, A. J., Codreanu, S. G., and Liebler, D. C. (2005) Sample preparation and digestion for proteomic analyses using spin filters. *Proteomics* **5,** 1742–1745
30. Wisniewski, J. R., Zougman, A., Nagaraj, N., and Mann, M. (2009) Universal sample preparation method for proteome analysis. *Nat. Methods* **6,** 359–362
31. Erde, J., Loo, R. R., and Loo, J. A. (2014) Enhanced FASP (eFASP) to increase proteome coverage and sample recovery for quantitative proteomic experiments. *J. Proteome Res.* **13,** 1885–1895
32. Rappsilber, J., Ishihama, Y., and Mann, M. (2003) Stop and go extraction tips for matrix-assisted laser desorption/ionization, nanoelectrospray, and LC/MS sample pretreatment in proteomics. *Anal. Chem.* **75,** 663–670
33. Greco, T. M., Guise, A. J., and Cristea, I. M. (2016) Determining the composition and stability of protein complexes using an integrated label-free and stable isotope labeling strategy. *Methods Mol. Biol.* **1410,** 39–63
34. Choi, H., Larsen, B., Lin, Z. Y., Breitkreutz, A., Mellacheruvu, D., Fermin, D., Qin, Z. S., Tyers, M., Gingras, A. C., and Nesvizhskii, A. I. (2011) SAINT: probabilistic scoring of affinity purification-mass spectrometry data. *Nat. Methods* **8,** 70–73
35. Mellacheruvu, D., Wright, Z., Couzens, A. L., Lambert, J. P., St-Denis, N. A., Li, T., Miteva, Y. V., Hauri, S., Sardiu, M. E., Low, T. Y., Halim, V. A., Bagshaw, R. D., Hubner, N. C., Al-Hakim, A., Bouchard, A., Faubert, D., Fermin, D., Dunham, W. H., Goudreault, M., Lin, Z. Y., Badillo, B. G., Pawson, T., Durocher, D., Coulombe, B., Aebersold, R., Superti-Furga, G., Colinge, J., Heck, A. J., Choi, H., Gstaiger, M., Mohammed, S., Cristea, I. M., Bennett, K. L., Washburn, M. P., Raught, B., Ewing, R. M., Gingras, A. C., and Nesvizhskii, A. I. (2013) The CRAPome: a contaminant repository for affinity purification-mass spectrometry data. *Nat. Methods* **10,** 730–736
36. Shannon, P., Markiel, A., Ozier, O., Baliga, N. S., Wang, J. T., Ramage, D., Amin, N., Schwikowski, B., and Ideker, T. (2003) Cytoscape: a software environment for integrated models of biomolecular interaction networks. *Genome Res.* **13,** 2498–2504
37. Szklarczyk, D., Morris, J. H., Cook, H., Kuhn, M., Wyder, S., Simonovic, M., Santos, A., Doncheva, N. T., Roth, A., Bork, P., Jensen, L. J., and von Mering, C. (2017) The STRING database in 2017: quality-controlled protein-protein association networks, made broadly accessible. *Nucleic Acids Res.* **45,** D362–D368
38. Bindea, G., Mlecnik, B., Hackl, H., Charoentong, P., Tosolini, M., Kirilovsky, A., Fridman, W. H., Pages, F., Trajanoski, Z., and Galon, J. (2009) ClueGO: a Cytoscape plug-in to decipher functionally grouped gene ontology and pathway annotation networks. *Bioinformatics* **25,** 1091–1093
39. Metsalu, T., and Vilo, J. (2015) ClustVis: a web tool for visualizing clustering of multivariate data using Principal Component Analysis and heatmap. *Nucleic Acids Res.* **43,** W566–W570
40. Tyanova, S., and Cox, J. (2018) Perseus: A Bioinformatics Platform for Integrative Analysis of Proteomics Data in Cancer Res. *Methods Mol. Biol.* **1711,** 133–148
41. Jacobsen, J. C., Gregory, G. C., Woda, J. M., Thompson, M. N., Coser, K. R., Murthy, V., Kohane, I. S., Gusella, J. F., Seong, I. S., MacDonald, M. E., Shioda, T., and Lee, J. M. (2011) HD CAG-correlated gene expression changes support a simple dominant gain of function. *Hum. Mol. Genet.* **20,** 2846–2860
42. Miteva, Y. V., Budayeva, H. G., and Cristea, I. M. (2013) Proteomics-based methods for discovery, quantification, and validation of protein-protein interactions. *Anal. Chem.* **85,** 749–768
43. Mayeda, A., Badolato, J., Kobayashi, R., Zhang, M. Q., Gardiner, E. M., and Krainer, A. R. (1999) Purification and characterization of human RNPS1: a general activator of pre-mRNA splicing. *EMBO J.* **18,** 4560–4570
44. Elvira, G., Massie, B., and DesGroseillers, L. (2006) The zinc-finger protein ZFR is critical for Staufen 2 isoform specific nucleocytoplasmic shuttling in neurons. *J. Neurochem.* **96,** 105–117
45. Schobel, S., Neumann, S., Hertweck, M., Dislich, B., Kuhn, P. H., Kremmer, E., Seed, B., Baumeister, R., Haass, C., and Lichtenthaler, S. F. (2008) A novel sorting nexin modulates endocytic trafficking and alpha-secretase cleavage of the amyloid precursor protein. *J. Biol. Chem.* **283,** 14257–14268
46. Zhu, Y., Kakinuma, N., Wang, Y., and Kiyama, R. (2008) Kank proteins: a new family of ankyrin-repeat domain-containing proteins. *Biochim. Biophys. Acta* **1780,** 128–133
47. Gomez, T. S., and Billadeau, D. D. (2009) A FAM21-containing WASH complex regulates retromer-dependent sorting. *Dev. Cell* **17,** 699–711
48. Marat, A. L., and Haucke, V. (2016) Phosphatidylinositol 3-phosphates-at the interface between cell signalling and membrane traffic. *EMBO J.* **35,** 561–579
49. Guise, A. J., Greco, T. M., Zhang, I. Y., Yu, F., and Cristea, I. M. (2012) Aurora B-dependent regulation of class IIa histone deacetylases by

mitotic nuclear localization signal phosphorylation. *Mol. Cell. Proteomics* **11,** 1220–1229
50. McColgan, P., and Tabrizi, S. J. (2018) Huntington's disease: a clinical review. *Eur. J. Neurol.* **25,** 24–34
51. Wang, N., Gray, M., Lu, X. H., Cantle, J. P., Holley, S. M., Greiner, E., Gu, X., Shirasaki, D., Cepeda, C., Li, Y., Dong, H., Levine, M. S., and Yang, X. W. (2014) Neuronal targets for reducing mutant huntingtin expression to ameliorate disease in a mouse model of Huntington's disease. *Nat. Med.* **20,** 536–541
52. Jia, D., Gomez, T. S., Metlagel, Z., Umetani, J., Otwinowski, Z., Rosen, M. K., and Billadeau, D. D. (2010) WASH and WAVE actin regulators of the Wiskott-Aldrich syndrome protein (WASP) family are controlled by analogous structurally related complexes. *Proc. Natl. Acad. Sci. U.S.A.* **107,** 10442–10447
53. Duan, W., Jiang, M., and Jin, J. (2014) Metabolism in HD: still a relevant mechanism? *Mov. Disord.* **29,** 1366–1374
54. Raymond, L. A. (2017) Striatal synaptic dysfunction and altered calcium regulation in Huntington disease. *Biochem. Biophys. Res. Commun.* **483,** 1051–1062
55. Yao, Y., Cui, X., Al-Ramahi, I., Sun, X., Li, B., Hou, J., Difiglia, M., Palacino, J., Wu, Z. Y., Ma, L., Botas, J., and Lu, B. (2015) A striatal-enriched intronic GPCR modulates huntingtin levels and toxicity. *Elife* 4
56. Song, H., Li, H., Guo, S., Pan, Y., Fu, Y., Zhou, Z., Li, Z., Wen, X., Sun, X., He, B., Gu, H., Zhao, Q., Wang, C., An, P., Luo, S., Hu, Y., Xie, X., and Lu, B. (2018) Targeting Gpr52 lowers mutant HTT levels and rescues Huntington's disease-associated phenotypes. *Brain* **141,** 1782–1798
57. De Souza, E. B., Whitehouse, P. J., Folstein, S. E., Price, D. L., and Vale, W. W. (1987) Corticotropin-releasing hormone (CRH) is decreased in the basal ganglia in Huntington's disease. *Brain Res.* **437,** 355–359
58. Valor, L. M. (2017) Understanding histone deacetylation in Huntington's disease. *Oncotarget* **8,** 5660–5661
59. Louis Sam Titus, A. S. C., Yusuff, T., Cassar, M., Thomas, E., Kretzschmar, D., and D'Mello, S. R. (2017) Reduced expression of Foxp1 as a contributing factor in Huntington's disease. *J. Neurosci.* **37,** 6575–6587
60. Doyon, Y., Selleck, W., Lane, W. S., Tan, S., and Cote, J. (2004) Structural and functional conservation of the NuA4 histone acetyltransferase complex from yeast to humans. *Mol. Cell. Biol.* **24,** 1884–1896
61. Suganuma, T., Gutierrez, J. L., Li, B., Florens, L., Swanson, S. K., Washburn, M. P., Abmayr, S. M., and Workman, J. L. (2008) ATAC is a double histone acetyltransferase complex that stimulates nucleosome sliding. *Nat. Struct. Mol. Biol.* **15,** 364–372
62. Schulze, J. M., Wang, A. Y., and Kobor, M. S. (2010) Reading chromatin: insights from yeast into YEATS domain structure and function. *Epigenetics* **5,** 573–577
63. Dhalluin, C., Carlson, J. E., Zeng, L., He, C., Aggarwal, A. K., and Zhou, M. M. (1999) Structure and ligand of a histone acetyltransferase bromodomain. *Nature* **399,** 491–496
64. Sharma, K., Schmitt, S., Bergner, C. G., Tyanova, S., Kannaiyan, N., Manrique-Hoyos, N., Kongi, K., Cantuti, L., Hanisch, U. K., Philips, M. A., Rossner, M. J., Mann, M., and Simons, M. (2015) Cell type- and brain region-resolved mouse brain proteome. *Nat. Neurosci.* **18,** 1819–1831
65. Zhang, B., Wang, J., Wang, X., Zhu, J., Liu, Q., Shi, Z., Chambers, M. C., Zimmerman, L. J., Shaddox, K. F., Kim, S., Davies, S. R., Wang, S., Wang, P., Kinsinger, C. R., Rivers, R. C., Rodriguez, H., Townsend, R. R., Ellis, M. J., Carr, S. A., Tabb, D. L., Coffey, R. J., Slebos, R. J., Liebler, D. C., and Nci, C. (2014) Proteogenomic characterization of human colon and rectal cancer. *Nature* **513,** 382–387
66. Seaman, M., and Freeman, C. L. (2014) Analysis of the Retromer complex-WASH complex interaction illuminates new avenues to explore in Parkinson disease. *Commun. Integr. Biol* **7,** e29483
67. Valdmanis, P. N., Meijer, I. A., Reynolds, A., Lei, A., MacLeod, P., Schlesinger, D., Zatz, M., Reid, E., Dion, P. A., Drapeau, P., and Rouleau, G. A. (2007) Mutations in the KIAA0196 gene at the SPG8 locus cause hereditary spastic paraplegia. *Am. J. Hum. Genet.* **80,** 152–161
68. Lee, S., Chang, J., and Blackstone, C. (2016) FAM21 directs SNX27-retromer cargoes to the plasma membrane by preventing transport to the Golgi apparatus. *Nat. Commun.* **7,** 10939
69. Silva, F. R., Miranda, A. S., Santos, R. P. M., Olmo, I. G., Zamponi, G. W., Dobransky, T., Cruz, J. S., Vieira, L. B., and Ribeiro, F. M. (2017) N-type Ca(2+) channels are affected by full-length mutant huntingtin expression in a mouse model of Huntington's disease. *Neurobiol. Aging* **55,** 1–10
70. Gruber, S., Haering, C. H., and Nasmyth, K. (2003) Chromosomal cohesin forms a ring. *Cell* **112,** 765–777
71. Dorsett, D. (2007) Roles of the sister chromatid cohesion apparatus in gene expression, development, and human syndromes. *Chromosoma* **116,** 1–13
72. Krantz, I. D., McCallum, J., DeScipio, C., Kaur, M., Gillis, L. A., Yaeger, D., Jukofsky, L., Wasserman, N., Bottani, A., Morris, C. A., Nowaczyk, M. J., Toriello, H., Bamshad, M. J., Carey, J. C., Rappaport, E., Kawauchi, S., Lander, A. D., Calof, A. L., Li, H. H., Devoto, M., and Jackson, L. G. (2004) Cornelia de Lange syndrome is caused by mutations in NIPBL, the human homolog of Drosophila melanogaster Nipped-B. *Nat. Genet.* **36,** 631–635
73. Fujita, Y., Masuda, K., Bando, M., Nakato, R., Katou, Y., Tanaka, T., Nakayama, M., Takao, K., Miyakawa, T., Tanaka, T., Ago, Y., Hashimoto, H., Shirahige, K., and Yamashita, T. (2017) Decreased cohesin in the brain leads to defective synapse development and anxiety-related behavior. *J. Exp. Med.* **214,** 1431–1452
74. Neuwald, A. F., and Hirano, T. (2000) HEAT repeats associated with condensins, cohesins, and other complexes involved in chromosome-related functions. *Genome Res.* **10,** 1445–1452
75. Greco, T. M., Yu, F., Guise, A. J., and Cristea, I. M. (2011) Nuclear import of histone deacetylase 5 by requisite nuclear localization signal phosphorylation. *Mol. Cell. Proteomics* 10, M110.004317
76. Watkin, E. E., Arbez, N., Waldron-Roby, E., O'Meally, R., Ratovitski, T., Cole, R. N., and Ross, C. A. (2014) Phosphorylation of mutant huntingtin at serine 116 modulates neuronal toxicity. *PLoS ONE* **9,** e88284
77. Arbez, N., Ratovitski, T., Roby, E., Chighladze, E., Stewart, J. C., Ren, M., Wang, X., Lavery, D. J., and Ross, C. A. (2017) Post-translational modifications clustering within proteolytic domains decrease mutant huntingtin toxicity. *J. Biol. Chem.* **292,** 19238–19249
78. Mishra, R., Hoop, C. L., Kodali, R., Sahoo, B., van der Wel, P. C., and Wetzel, R. (2012) Serine phosphorylation suppresses huntingtin amyloid accumulation by altering protein aggregation properties. *J. Mol. Biol.* **424,** 1–14
79. Vizcaino, J. A., Cote, R. G., Csordas, A., Dianes, J. A., Fabregat, A., Foster, J. M., Griss, J., Alpi, E., Birim, M., Contell, J., O'Kelly, G., Schoenegger, A., Ovelleiro, D., Perez-Riverol, Y., Reisinger, F., Rios, D., Wang, R., and Hermjakob, H. (2013) The PRoteomics IDEntifications (PRIDE) database and associated tools: status in 2013. *Nucleic Acids Res.* **41,** D1063–D1069